TRANSIENT BEHAVIOUR
IN
GLUCOSE/OXYGEN BIOFUEL CELLS

By

HAN YAN, B.ENG.

A Thesis

Submitted to the School of Graduate Studies

In Partial Fulfillment of the Requirements

For the Degree

Master of Applied Science

McMaster University

MASTER OF APPLIED SCIENCE (2009) McMaster University

(Materials Science and Engineering) Hamilton, Ontario

TITLE: Transient Behaviour of Glucose/Oxygen Biofuel Cells

AUTHOR: Han Yan, B. Eng. (Mcmaster University)

SUPERVISOR: Professor Gu Xu

NUMBER OF PAGES: XIII, 80

H. Yan
Materials Science and Engineering

Abstract

In this thesis, solutions to the problem of low power density caused by pH deviation in anode and cathode of a glucose/oxygen based enzymatic fuel cell using GOx and FMCA are provided. Moreover, conclusive evidence of a large active area in this type of fuel cell is determined using a transient state study. The complete process of electrical double layers formation is described.

A survey of the solutions to low power density caused by pH deviation is conducted and two feasible alternatives are suggested. The first alternative, using Tris buffer with no alkaline ions resulted in even larger pH gradient. The second alternative: using anion exchange membrane (AEM) successfully reduced the pH gradient by introducing lower power density than the biofuel cells using a Nafion membrane. It was proven that the high internal resistance of the AEM is responsible for the drop in energy output of the biofuel cell.

A transient study was conducted on the biofuel cells in order to investigate the internal resistance of the components. A discrepancy was found when applying the rarely-mentioned internal circuit model to biofuel cells. The model predicted a much larger surface area for the electrode than was physically measured for the cells. It is therefore concluded that the proposed electrochemical double layers are in the electrolyte as well as on the interface. Finally, a detailed description of electron/proton double layer in the electrolyte associated with each reaction step is given, assuming that double layers can be found on the enzymes and mediators.

A complete list of requirements for equivalent circuit is portrayed for our glucose/oxygen enzymatic biofuel cell. The equivalent circuit suggests a possible direction for future biofuel cell research.

Acknowledgements

The author wishes to express his gratitude to Dr. Gu Xu for his experienced supervision throughout the thesis work. The discussions were always helpful and full of valuable ideas.

The author would like to thank Dr. Ma from Nanjing Normal University for her discussion and questioning through committee meeting.

Very special thanks must be given to Xinxin Zhao for her invaluable discussion and great help.

The author would also like to thank Stephen Jones. His confidence and support of the research is greatly appreciated

The author would like to thank his group members, Kewei Wang and Feihong Nan, for their helpful advice and assistance with this project.

The author wishes to thank his friends, Zhixin Jiang and He Ren for their constant support especially during his ankle injury at the beginning of project.

The financial support from INCO and McMaster University is greatly appreciated.

Finally, the author wishes to express deep gratitude to my parents, Keqiang Yan and Ailing Li, for their constant encouragement and assistant throughout my study.

Table of Contents

Abstract i
Acknowledgement ii
Table of Contents iii
Table of Figures vi
Table of Tables viii
1. Introduction 1
1.1. Definition of a Biofuel Cell 1
1.2. History of Biofuel Cells 2
1.3. Working Principle of Biofuel Cells 3
1.4. Microbial Fuel Cells 5
1.5. Enzymatic Fuel Cells 8
1.5.1. Enzyme Stability/Activity 8
1.5.2. Enzymes Types 9
1.5.3. Electron Transfer 11
1.6. Brief Comparison of Microbial/Enzymatic BFC 12
1.7. Future Application of Biofuel Cells 13
1.8. Problem Statement 14
1.9. Thesis Overview 15
2. Literature Review 16
2.1. Levels of Analysis on Biofuel cells 16
2.1.1. Electro-Biochemistry 17
2.1.2. Thermodynamics 17
2.1.3. Steady State Behaviour 20
2.1.4. Transient Behaviour 21
2.2. Overpotential 22
2.2.1. Activation Overpotential 22
2.2.1.1. Tafel Relation 22
2.2.1.2. Electrochemical Double Layer 24
2.2.1.3. Electron Transfer and Efficiency Loss 24
2.2.2. Ohmic Overpotential 25
2.2.3. Concentration Overpotential 25
2.2.4. Summary of Overpotential 27
2.3. Proton Transport and pH Gradient for Low Power Density 27
2.3.1. Protons' Driving Force in Nafion 27
2.3.2. Modes of Proton Transfer in Membrane 28
2.3.2.1. Introduction to Nafion 28

Table of Figures

Figure 1.1 Enzymatic biofuel cells 4
Figure 1.2 Electron transfer in enzymatic biofuel cells 5
Figure 1.3 Stability: (1) hydrogenase CFM electrode, (2, 3) soluble hydrogenase in solution, (3) soluble hydrogenase with stabilizer (sodium azide 0.2%) 9
Figure 1.4 Different locations of enzyme active sites. (A) Diffusional active sites. (B) Active sites located on the periphery. (C) Active sites surrounded by protein shell [2] 10
Figure 1.5 Electron-transfer mechanisms. (a) Direct electron transfer (b) Electron transfer via redox mediator [14] 11
Figure 1.6 Implanted biofuel cells directly attached to a blood vessel 13
Figure 2.1 Structure of β-D-glucose(left) and δ-D-gluconolactone (right) [28] 17
Figure 2.2 Typical voltage/current curve for low temperature/normal atmosphere fuel cell [33] 20
Figure 2.3 Typical Tafel plot for fast/slow reactions 22
Figure 2.4 Electrochemical double layer 24
Figure 2.5 Concentration profile near electrode surface 26
Figure 2.6 Performance of a glucose/O_2 biofuel cell [40] 27
Figure 2.7 The Bridge model of oxygen reduction [41] 28
Figure 2.8 Structure of Nafion [42] 29
Figure 2.9 pH and glucose oxidase activity 31
Figure 2.10 Structure of $TrisH^+$/Tris buffer [52] 37
Figure 2.11 Electrode structure of PEM fuel cells [53] 40
Figure 2.12 An equivalent circuit model of a PEM fuel cell [33] 40
Figure 2.13 Schematic illustration of voltage vs. time plot during a current interruption experiment.. 41
Figure 2.14 Set-up for load switch test 42
Figure 3.1 Schematic Diagram of our biofuel cell 44
Figure 3.2 Molecular Structure of Ferrocene monocarboxylic acid (FMCA) [24] 45
Figure 3.3 Schematic of our biofuel cell's operation and measurement apparatus 47
Figure 4.1 pH in a Nafion based enzymatic fuel cell and time 50
Figure 4.2 Current, power output and time in a Nafion based enzymatic fuel cell 50
Figure 4.3 pH in a Tris buffer based biofuel cell and time 51
Figure 4.4 pH in an AEM based enzymatic fuel cell and time 53
Figure 4.5 Open circuit voltage and time 54
Figure 4.6 Voltage and current density 55
Figure 4.7 Power density and current density 55
Figure 4.8 Nyquist plot for all membranes 57
Figure 4.9 Proposed internal circuit for biofuel cells [61] 58

Figure 4.10 Basic RC circuit model during charge 59
Figure 4.11 Load step measurement for all membranes at 18 degrees Celsius 61
Figure 4.12 Time constant 1 for all membranes at 18 degrees Celsius 61
Figure 4.13 Time constant 2 for all membranes at 18 degrees Celsius 62
Figure 4.14 Polarization curve and load step test 62
Figure 4.15 GOx activity and temperature [67] 65
Figure 4.16 Step load measurement for Nafion at 18 and 30 degrees Celsius 66
Figure 4.17 Time constants 1 for Nafion at 18 and 30 degrees Celsius 66
Figure 4.18 Time constants 2 for Nafion at 18 and 30 degrees Celsius 66
Figure 4.19 Step load measurement for Snowpure at 18 and 30 degrees Celsius 67
Figure 4.20 Time constants 1 for Snowpure at 18 and 30 degrees Celsius 67
Figure 4.21 Time constants 2 for Snowpure at 18 and 30 degrees Celsius 67
Figure 4.22 Internal energy drop in a PEM fuel cell 69
Figure 4.23 Transient charge distributions in a PEM fuel cell without external circuit 70
Figure 4.24 Internal charge distributions in a PEM fuel cell with external circuit 71
Figure 4.25 Energy drop in a Glucose/oxygen enzymatic biofuel cell 73

Table of Tables

Table 2.1 Standard Gibbs energies of formation $\Delta_f G°$ at 25°C, pH 7 [32] 19
Table 4.1 Overall resistances for different membranes 56
Table 4.2 Time constant and capacitance for all membranes at 18 degrees Celsius 63
Table 4.3 Time constants and capacitance for Nafion and Snowpure at 18 and 30 degrees Celsius 68

1. Introduction

1.1. Definition of a Biofuel Cell

Biological fuel cell, abbreviated as biofuel cell, is an energy conversion device that converts chemical energy into electrical energy via electrochemical reactions including biological pathways [1]. The term biological stems from the fact that energy-abundant fuels and the catalysts used in the cells are all biological substances. The substrates for oxidation reaction, namely methanol, organic acids and glucose; are abundant, renewable and can all be produced by biological metabolisms. For these reasons biological fuel cells hold promise in the long term for energy production [2].

During the 20^{th} century, energy consumption has increased dramatically and there is no sign that this trend will abate in the near future. Additionally, the irreversible damage to the environment caused by over-consumption of fossil fuel is a cause for concern among the public. A fuel cell, an electrochemical conversion device, has been considered as an alternative to some of the energy-related problems. In a typical PEM (proton exchange membrane) fuel cell, hydrogen gas is split into protons and electrons aided by platinum catalyst. The polymer electrolyte membrane, an alternative name for PEM, allows only the positively charged ions to pass through. At the same time, the negatively charged electrons must travel through the external circuit, creating an electrical current. In the cathode, protons and oxygen recombine to form water. Fuel cells gain their reputation for clean off-gas, simple structure, high efficiency and low noise. The main difference between a fuel cell and a heat engine is that the latter doesn't involve a low-efficiency energy conversion process: from chemical energy to heat and then mechanical energy. The main difference between a fuel cell and battery or a supercapacitor is that the latter two store electrical energy chemically in a closed

system. A fuel cell can operate virtually continuously as long as the necessary fuel flows are maintained.

PEM Fuel cells are commercially available from several watt output to several hundred watt hydrogen engine used in urban transportation systems [3]. Theoretically, the off-gas for a PEM fuel cell is pure water, a substance that does no harm to environment. The use of hydrogen gas, which is derived from hydrocarbons, as a fuel when we are approaching the depletion of fossil fuel resources, is an obstacle to a wide application of PEM fuel cells. Hydrogen production, hydrogen storage, and the use of an expensive catalyst (platinum) remain the three major obstacles yet to be overcome by PEM fuel cells research. However, the biofuel cells overcome the previous three problems by its nature, using renewable biomass as fuel and microorganism or enzyme as catalyst.

1.2. History of Biofuel Cells

The name of bioelectricity was first introduced in the late 18th century when Luigi Galvani observed the twitching of a frog leg [3]. The real start of biofuel cells can be dated back to 1910, when Dr. Michael Cress Potter, a professor of botany at the University of Durham demonstrated current and voltage generated from organisms. In the 1960s, biofuel cells became popular for the first time in the history because NASA intended to turn organic waste into electricity on its space flights. Commercially available biofuel cells were first made in 1963 as power source in some appliances at sea. Unfortunately, photovoltaics, another energy conversion device, took the place of biofuel cells in NASA's space flight because of its inexhaustible fuel. Biofuel cells thus lost the commercial value in the civilian market because of the lack of research investment. Interest in the development of biofuel cells later revived in the 70s and 80s because of the oil crisis. In 1969 Yao et al. [4] announced that glucose could be used as an anode and as a fuel. This observation is of historical importance

with respect to this thesis, as it demonstrated the use of glucose as a fuel. Also, the concept of a mediator was introduced in order to enhance the efficiency of biofuel cells with various microorganisms. They showed that a mediator could enhance both the efficiency of electron-transfer and the reaction rate. This important step was contributed by Bennetto et al. [5] [6] and it is also a pertinent topic in our research. Later in the end of 20^{th} century and the beginning of 21^{th} century, researchers in this area tried different combinations of biological catalysts and mediators to enhance biofuel cells' performance. Another group of researchers dedicated their time looking for appropriate and efficient ways to wire the catalysts onto the electrode, in order to promote electron transfer. Currently, the maximum power density of a biofuel cell is at the range of 0.1 to 1 mW/cm^2 [7]. This value is 1000 times lower than that of the typical PEM fuel cell available on the commercial market [8]. A recent study by Rabaey et al. [9] reported for a microbial biofuel cell the highest known power density value of 0.36 mW/cm^2. The largest power density reported for enzymatic type biofuel cells was 0.46mW/cm^2 [10]. SONY in 2007 announced the development of a "sugar-cell" using glucose and various mediators and enzymes in a system with membrane [11]. The output power was 50mW (1.5 mW/cm^2), which was enough to power a portable mp3 player. The size of the battery was 40 ml and the electricity was generated by injecting concentrated glucose/sugar into the case.

1.3. Working Principle of Biofuel Cells

As mentioned in the history of biofuel cells, glucose and mediator were consequently introduced into the research of biofuel cells in late of last century. We adopt this combination using specifically 2β - D-glucose as fuel and glucose oxidase as anodic catalyst. The basic chemical equation is listed as follows:

Anode: 2β - D-glucose $\rightarrow$ 2δ – gluconolactone + $4e^-$ + $4H^+$ (1.1)

Cathode: $O_2 + 4H^+ + 4e- \rightarrow 2H_2O$ (1.2)

Therefore, the whole reaction can be written as:

$$2\beta\text{ - D-glucose} + O_2 \rightarrow 2H_2O + 2\delta - \text{gluconolactone} \quad (1.3)$$

For different biofuel cells that depend on different anodic fuels, the equations varied. However, all governing equations share the same mechanism: electrons are transferred by the external circuit while protons migrate to cathode in the internal circuit. Both electrons and protons travel from anode to cathode and recombine with oxygen to form water in cathode. Internally, protons flow through a proton exchange membrane, which is as same as the one used in hydrogen PEM fuel cells. The process is schematically illustrated in figure 1.1 below:

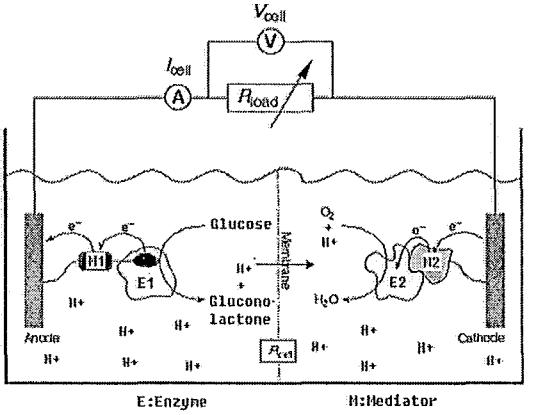

Figure 1.1 Enzymatic biofuel cells

Electron transfer mediators (M), both found in anode and cathode in figure 1 are introduced to obtain higher electron transfer rate and efficiency. The transportation of electrons in external circuit triggers current, and therefore makes a biofuel cell an energy device. Figure above gives a brief idea how an enzymatic type of biofuel cell works. Biological reactions are not necessarily found in both anode and cathode of a biofuel cell because a biofuel cell with only anodic biological reaction can significantly reduce the complexity of the system.

Consequently the working of a biofuel cell can be illustrated by the following steps: fuel oxidation, proton transportation, electron transportation and reduction of

oxidant. Essentially any published literature focuses any combinations of these steps.

There exists two types of catalysts used in biofuel cells: enzymatic or microbial. In a microbial fuel cell, the mechanism is similar to that of enzymatic biofuel cell, except that the substances used to catalyze the reactions are whole microorganisms instead of enzymes. Sections 1.4 and 1.5 will discuss both types of cell in more detail.

1.4. Microbial Fuel Cells

Back in the 1970s, microbial fuel cells were explored in concept [12]. In 2006 Logan et al. [21] provided an overall picture on how microbial fuel cell worked in a review paper.

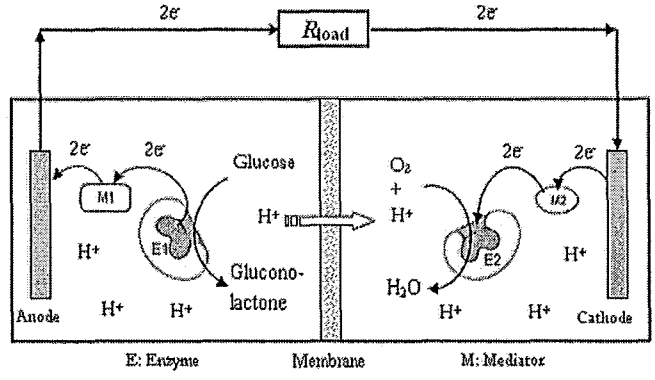

Figure 1.2 Electron transfer in enzymatic biofuel cells

Due to their low power density and sophisticated reaction, microbial fuel cells were first utilized in domestic wastewater treatment in 1991 [13]. Recently, microbial fuel cells with higher power density up to 0.36mW/cm^2 were developed and this enhanced power output provides many more possible opportunities for practical applications other than wastewater treatment. Biofuel cells can be divided into 3 categories according to the way they produce electricity, either direct or indirect, according to Shukla et al. [1].

1) Integrated bioreactor microbial biofuel cells

In this system, a bioreactor is always connected with a conventional fuel cell in

series. Hydrogen gas produced by microbiological fermentation goes directly into anode of a fuel cell. Even by using a highly efficient microorganism, C.butyricum, the biomass to hydrogen conversion rate is more than three orders of magnitude lower than is required by the adjacent fuel cell [14]. Gas impurities such as CO and H_2S produced in addition to hydrogen would poison the catalysts in the fuel cell and therefore limit the fuel cell performance. Low rate of hydrogen production as well as gas contamination do not make this a promising biofuel cell technology.

In a slightly different case, fuels including all by-products such as formic acid, lactic acid, sulphion and sulphides are oxidized in the fuel cell. However, the interaction between bacterial in the fermentation cell and sulphides or sulphion species has negative effect on the biological reaction. Moreover, sulphion species poison most metallic electrodes which are often used in conventional fuel cells. These two effects combined together result in both poor kinetic and efficiency performance.

2) The microbial fuel cells with direct electron transfer

Direct electron transfer (DET) in biofuel cells, is essentially the process of electron motion from electrolyte to anode without using any medium. At the anode, unlike PEM fuel cells, biological reactions are in a liquid electrolyte and therefore make electron transfer a difficult step. Mediatorless biofuel cells have advantage over the biofuel cells with mediator in terms of cost. In contrast, it also limits the types of fuels to simple organic acids. For instance, S. putrefacien IR-1 mediatorless microbial cell, prepared by Kim et al. [16] can provide 0.04mA current with a 1000 ohms external load using only lactate and pyruvate. Recently, microorganisms cultured in biofuel cells using wastewater as substrate have shown very high energy conversion activity. Clostrdium EG3 microbial fuel cell prepared by Park et al. [17] and A. hydrophila PA3 microbial fuel cell prepared by Pham et al. [18] have achieved high performance: 0.22mA and 1.8mA respectively. All these progresses make mediatorless biofuel cells a promising route in microbial fuel cells research.

3) The microbial fuel cells using mediators

In this configuration, electron-transfer mediators shuttle electrons between the microbe and the electrode. The mediator molecules accept electrons from the biological electron transport chain of the microorganisms and transport them to the anode of the biofuel cell.

Microbial membranes, the layers on the surface of microorganisms, hinder direct and efficient electrical transfer. Mediators, such as Thionine, naphthodiazine and some organic dyes, have been introduced to shuttle electrons. Using mediators, however, adds complexity to the microbial fuel cell system. Instead of the simple mode of electron transfer, the electrochemical rate-constant of mediators' reoxidation must be taken into account.

Researchers have been attempting to use mixtures of multiple mediators to form mediator groups; this has proven to be efficient. A mixture of Thionine and Fe(III) EDTA (define) as mediators in a glucose based system shows better overall power output than using any one component [19].

According to the working mechanism of mediators, the mediators are to be attached to the surface of the microorganism to attain better connection with the active site inside the center of the microorganisms.

The mediators can be coupled to the microorganisms in three ways: a) as diffusional mediators shuttling between the microbial suspension and the anode surface; b) diffusional mediators shuttling between the anode and microbial cells covalently linked to the electrode; c) mediators absorbed on the microbial cells.

A mixture of substrates also provides an ideal environment for microorganism because they may have multiple oxidation mechanisms. For example, domestic wastewater has been pointed out as a potential fuel for microbial fuel cell with high power output by Kim et al. [20].

1.5. Enzymatic Fuel Cells

Using enzymes as catalyst originates from a desire to have specific and defined reactions in the fuel cells. The enzymes responsible for the desired process can be separated and purified from living organisms. Some interesting aspects of enzymatic fuel cells should be reviewed as an introduction to this biofuel cell study. Many of the aspects of enzymatic catalysts are as same as those for microbial cells, such as electron transfer between enzyme and electrode surface. However, some aspects are distinctive for enzymatic fuel cells, such as the selection of enzymes, the enzymes' activity and stability.

1.5.1. Enzyme Stability/Activity

Enzymes are biologically fragile due to the fact that they are proteins that selectively react to their substrates and they speed up only a few reactions among many possibilities. Therefore the activity of the enzyme is also severely affected by temperature, chemical environment (*e.g.*, pH), and the concentration of the substrate. As an example, Glucose Oxidase (GOx), the enzyme used in our experiment, shows the best performance at 30 degrees Celsius and neutral pH (=7). A detailed discussion on enzyme stability and activity will be included in the literature review.

Stability, however, is not the only function of activity, but also depends on the life time of a specific enzyme. The life time of an enzyme, which eventually determines life time of a biofuel cell, is also affected by the configuration for a given application. For example, Kim et al. [22] found that by immobilizing hydrogenase, an enzyme used for glucose oxidation, half of its activity was preserved after half a year. However, it was found that the enzyme lost its activity by being dissolved in water. Schematically, the dependence of activity decay with respect to the electrolyte is illustrated below in figure 1.3 by Karyakin et al. [23]. The y-axis, ranging from 0 to 100%, quantitatively represents the relative activity of a specific enzyme.

Biochemically, absolute activity of enzymes are defined as the amount of enzyme that oxidizes 1 μ mol of substrate material at pH=7.0 and 25 degrees Celsius. Correspondingly, relative activity is the ratio of the amount of enzyme that needs to oxidize 1 μ mol of substrate material at the condition above over the amount at any specific condition. Being a catalyst, enzymes keep the same chemical structure before and after the oxidation reaction. The role of enzyme in this particular reaction is as the medium which transfers the electron from the substrate to the cathode. Therefore, in the definition of relative activity of the enzymes, the term "oxidize" doesn't result in the "reduction" of enzyme. The relative activity of an enzyme is also influenced by the way they are immobilized. For instance, Tetrabutylammonium bromide modified Nafion membrane was used to entrap dehydrogenase as shown by Moore et al. [25] in 2004. They claimed that the fuel cells showed no significant power decay during several weeks of continuous operation.

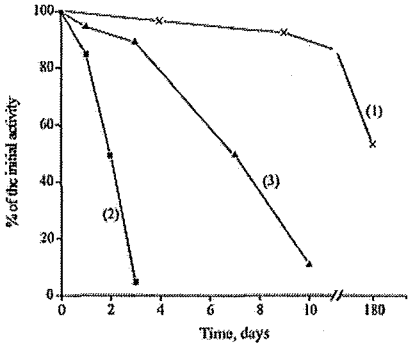

Figure 1.3 Stability: (1) hydrogenase CFM electrode, (2, 3) soluble hydrogenase in solution, (3) soluble hydrogenase with stabilizer (sodium azide 0.2%)

1.5.2. Enzymes Types

The active sites responsible for electron transfer are located inside enzymes. Efficient electron transfer has nothing to do with the protein matrices which surround it. According to the positions of their electron-transfer unit, enzymes can be divided into 3 groups. Unfortunately, the types are not clearly defined as some of enzymes are associated with more than one group below.

First group of enzymes are those with active sites weakly bounded to the protein of the enzyme. Examples are nicotinamide adenine dinucleotide phosphate couple (NADH/NAD+), a coenzyme present in most living cells and derived from the B vitamin nicotinic acid. They serve as reductants in various metabolic processes. The active center can diffuse out of the enzymes during electron transfer and therefore can play the role of mediator as well.

In the second group, at least part of the active center is conveniently located at or near the periphery of the protein shell. Some peroxidases are examples of this group. The structure makes direct electron acceptance or release possible. The way of orienting the enzymes on electrode for optimized activity is a crucial challenge associated with this type of enzyme.

The last group of enzymes deeply bound active sites in a protein or glycoprotein shell. In this case, direct electron transfer from the redox center to the electrode is extremely slow or even negligible. Flavin Adenine Dinucleotide (FAD) for example, requires the use of mediator molecules capable of penetrating into the enzyme to realize electron transfer.

Schematically, all 3 groups of enzymes are described by Bullen et al. in 2006 [2].

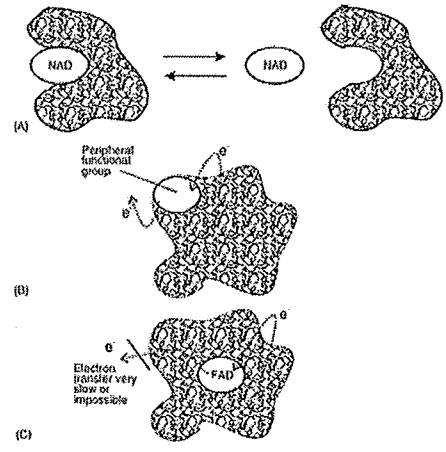

Figure 1.4 Different locations of enzyme active sites. (A) Diffusional active sites. (B) Active sites located on the periphery. (C) Active sites surrounded by protein shell [2]

1.5.3. Electron Transfer

According to the types of enzymes listed above, direct electron transfer (DET) is a possible reaction mechanism. However, for the case of active sites being surrounded by the protein shell, mediator electron transfer (MET) must be utilized. Direct electron transfer versus mediator electron transfer is schematically illustrated below by Barton [14] in figure 1.5.

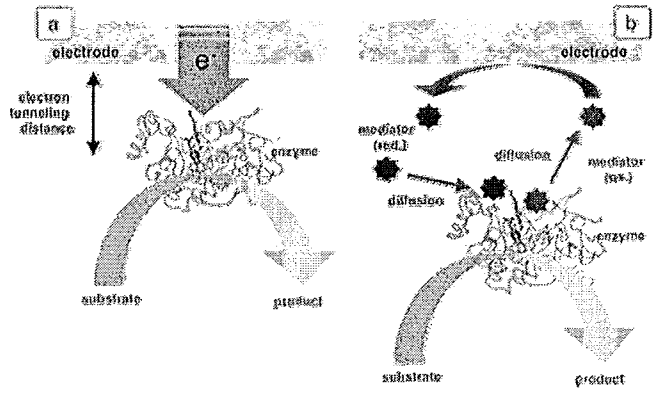

Figure 1.5 Electron-transfer mechanisms. (a) Direct electron transfer (b) Electron transfer via redox mediator [14]

DET has been observed for few enzymes, such as cytochrome *c*, laccase, hydrogenase, and several peroxidases. In DET, enzymatic and electrode reactions are coupled without the presence of mediators; the electrons are transferred directly from the substrate to the electrode. Electron transfer relies solely on the active site of the enzyme. As described in section 1.5.2, the enzyme's active site can diffuse outside the enzyme and this intrinsic property of the first group enzyme makes DET a possible reaction route.

The description above of the DET reaction is a simplified case. In reality, in many cases, DET is hindered by the thick and nonconductive protein shell that hosts the active site of an enzyme. To overcome this barrier, redox mediators are introduced to facilitate the transportation of electrons. According to figure 1.5 above, the mediator was in oxidized form before it travels to enzyme surface. On receiving the electron produced by enzymes in earlier step, the mediator is reduced, and travels towards the

surface of electrode. The mediator goes back to enzymes again in the original oxidized form after it transfers the extra electron to electrode. The driving force for electron transfer in the mediator is the potential difference caused by electrochemical reaction. The applicable mediator should be one whose redox potential is close to the enzymes redox potential. Schematically, the potential window of a mediator should lie between the potential windows of the overall biochemical reaction (including redox potential of enzymes). Of course, in order to minimize the potential loss caused by mediators, the potentials of ideal mediators should be as close to the potentials of enzymes as possible. The open-circuit potential of a glucose-oxygen biofuel cell, the type we focus on in this thesis, is primarily determined by the difference in redox potential of the two mediator couples if other sources of potential loss are neglected.

1.6. Brief Comparison of Microbial/Enzymatic BFC

Microbial fuel cells are based on living microbes and therefore have theoretically unlimited life time as long as fuel supply is maintained. Enzymatic fuel cells suffer from limited lifetime caused by depletion of enzymes. The rate of degradation and its relevant factors need to be well understood before biofuel cells are used commercially. Extraction of enzymes is much more expensive than growing bacteria or microorganisms on an artificial culture medium. In the case of enzymatic biofuel cells, research on small electrodes is deemed worthwhile because the proposed use for enzymatic cells is mostly for in vivo applications which demand a small but efficient electrode. In microbial systems however, the larger scale of electrodes and hence larger systems are explored. A high internal resistance arisen from microbial cell membranes is partly responsible for their low power density. However, enzymatic fuel cells are compatible with immobilization and wiring techniques and this provides a bright future for building devices with a high power density. Microbial biofuel cells, unlike enzymatic fuel cells, do not show selectivity on fuels and most fuels can be

fully oxidized. All these characteristics keep enzymatic fuel cells from being applied to wastewater treatment, which is considered an important application of biofuel cells.

1.7. Future Application of Biofuel Cells

Biofuel cells were once introduced into commercial market in the 1960s and lost market share gradually in the competition with other energy devices such as photovoltaics. After decades of research, they have redrawn people's attention in the late 20^{th} century.

The ultimate energy device which researchers have been working on is a PEM fuel cell using hydrogen fuel gas. Unlike hydrogen fuel cells, biofuel cells do not have any problem related to fuel storage. Theoretically, 5 kWh of electricity can be generated from one kilogram of glucose through complete oxidation. A mid-sized car, based on current market data available, could travel 10 kilometers using energy converted from only one kilograms of glucose. According to the power density researchers have achieved currently, the fuel efficacy is far from this theoretical limit.

Another promising application is an implantable device or sensor shown in figure 1.6 below. This type of cell may be used in a drug delivery system or as a blood sugar level sensor. The input to this type of cell would be glucose, a sugar found in the blood. Biological reactions are slow but stable for devices in the long run as the devices simulate biological metabolism inside human body.

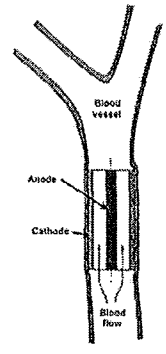

Figure 1.6 Implanted biofuel cells directly attached to a blood vessel

Another important application for microbial fuel cells is in the field of wastewater engineering. Microorganisms are capable of fully oxidizing multiple substances at a very low power density. If power density of the system is increased in the future, the cost of wastewater treatment can be offset by the energy generated using this cleaning process.

In 2007 SONY announced the development of an enzymatic "sugar-cell" using glucose and various mediators in a system with a membrane [26]. The total output power was 50mW (1.5 mW/cm^2), which was enough to power a portable mp3 player during the demonstration for a few seconds. However, SONY didn't mention the durability of the fuel cell, another key characteristic in order to make it commercialized.

1.8. Problem Statement

Biofuel cells have not been mass-produced even though they have been studied for nearly a century. The performance of biofuel cells, in terms of power density and lifetime, is much less than batteries/conventional fuel cells. 1 W/cm^2 is the typical power output for a platinum-based PEM fuel cell. The highest reported power output for a biofuel cell is still 2 to 3 orders of magnitude lower than that of a PEM fuel cell.

Many applications for biofuel cells require a power density of 10-100 mW/cm^2 at steady state. In order to fulfill this goal, a detailed characterization of the electron transfer as well as the internal resistance of the biofuel cell is necessary. Transient behaviour experiments reveal the very initial moments of the electrochemical reactions. Transient behaviour studies on all interfaces involved in the biofuel cell are the key to breaking the current bottlenecks in biofuel cell research. The transient behaviour as well as its internal equivalent circuit has been studied for PEM fuel cells intensely in the recent years. This thesis will discuss the transient behaviour and internal equivalent circuit of a glucose/oxygen based enzymatic biofuel cell.

1.9. Thesis Overview

The thesis consists of 5 Chapters. Chapter 1 provides very basic fundamentals of biofuel cells, including the definition, history, working principles and the basic problems of biofuel cells. In Chapter 2, a literature review is discussed; this includes previous research on the problem of low power output as well as some experimental techniques used by other researchers. Chapter 3 gives a detailed description of the experimental setup including chemicals, instruments and the ways in which the experiment were conducted. Chapter 4 provides the experimental results, analysis and discussion. Chapter 5 gives a brief summary of the work.

2. Literature Review

Several intensive literature reviews on biofuel cells have been published since the early 1990s. In 1999, Katz et al. [29] was the first group to review a non-compartmentalized biofuel cell using glucose/oxygen system. In 2006, Bullen et al. [2] reviewed all papers published since 1994 relating to biofuel cells. They classified all papers according to the nature of electrode reaction and biological reaction. In 2004, Barton et al. [14] published a systematic review on enzymatic biofuel cells, from the fundamentals of the mechanism for energy production to some of the engineering aspects relating to application of this technology. .

In 2006, Kim et al. [22] surveyed the challenges relating to the selection of biocatalysts for enzyme based biofuel cells. More papers relating to the problem of biofuel cells' low power density were published after 2007, including Rozendal et al.'s [31] report on a microbial fuel cell using different cation exchange membranes. The above reports of experimental and research results provide us with some novel ideas and pertinent information pertaining to experimental design.

2.1. Levels of Analysis on Biofuel cells

To obtain a better understanding of all the topics in biofuel cell research: from biological reaction to energy output, from proton transfer to electron transfer. It is necessary to review the entire biofuel cell step by step according to 4 levels of analysis: bio-electrochemistry, thermodynamics, steady state kinetics and transient behaviour.

2.1.1. Electro-Biochemistry

Because of the specific nature of chemistry, this paragraph will only focus on the chemistry of the reactions involved in our research: oxidation of glucose. Glucose is by far the most common carbohydrate and classified as: a monosaccharide, an aldose, a hexose, and a reducing sugar. A concentration of 60-100 mg/L glucose is found in human blood, this reminds us of one potential future application for the biofuel cells, a sugar sensor. The ring structure of glucose as illustrated in figure 1.7 [28], is oxidized through the aid of glucose oxidase. Glucose oxidase (GOx) is a small, stable enzyme that oxidizes only β-D-glucose to δ-D-gluconolactone. It is naturally found on the surface of fungi and inside honey. GOx is extracted by industrial fermentation of Aspergillus niger, a fungus, which is one of the most common species of genus Aspergillus.

During oxidation, each glucose molecule releases two protons, specifically the one bonded to the oxygen in the ring and the one from the secondary alcohol adjacent to the oxygen in the ring. To maintain conservation of charges, two electrons are released simultaneously. More precisely, according to equation (1.1) and (1.2), glucose oxidase only plays the role of catalyst and the substance that is indeed oxidizing β -D-glucose is oxygen.

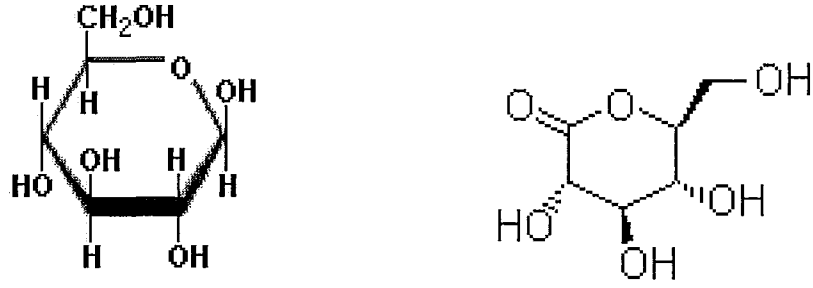

Figure 2.1 Structure of β -D-glucose(left) and δ -D-gluconolactone (right) [28]

2.1.2. Thermodynamics

Thermodynamics studies the conversion of energy from one form to another.

In the reversible reaction (1.1), (1.2) and (1.3), the theoretically available work is given by the equation:

$$W = nFE_r = -\Delta H - Q = -(\Delta H - T\Delta S) = -\Delta Gf \quad (2.1)$$

Where n is the number of electrons transferred per reactant molecule, F is Faraday constant, 96485 C/mol, E_r is the electromotive force (EMF) of the cell reaction, and ΔH is the enthalpy change.

The equation is based on a reversible system with no energy loss, and therefore the electrical work is equal to reduction in Gibbs free energy.

We can derive EMF according to equation (2.1) by

$$E_r = -\Delta Gf/nF \quad (2.2)$$

$-\Delta Gf$ here is the net Gibbs free energy of formation at a given temperature for the reaction (1.3) and is a function of the activities and temperatures of the reactants and products as shown by equation (2.3). Activities of all substances are denoted by a in equation (2.4).

$$\Delta Gf = \Delta Gf^{o} - RT\ln Q \quad (2.3)$$

$$Q = (a_{glucose}^{2}.aO_2)/(a_{gluconolatone}.aH_2O^2) \quad (2.4)$$

When the activities of all substance are equal to one, namely at the standard state (25 degrees Celsius and 1 atmosphere) for gas and the ionic strengths are equal for aqueous species, Q is equal to one. Eo is used to represent the EMF for a reaction at standard state and is used to solve for the actual EMF by the given equation:

$$Er = Eo + (RT/2F)\ln Q \quad (2.5)$$

Activity is a function of temperature, gas pressure and ionic strength (liquid only) for all reactants. Therefore the observed values of the Gibbs free energy of formation change for different conditions. The relationship between ionic strength and activity in solution is as follows:

$$I = 0.5\Sigma CiZi^2 \quad (2.6)$$

I is ionic strength, Ci is molar concentration of i_{th} ion present in the solution and Zi is its charge number.

$$\log f=(-0.51Z2\sqrt{I})/(1+\sqrt{I}) \quad (2.7)$$

In equation (2.7), f is the activity coefficient, a term that is used to calculate the relationship between activity a and concentration C_{ion} as shown in equation (2.8)

$$a=f\,C_{ion} \quad (2.8)$$

Equation (2.6), (2.7) and (2.8) provide a good estimation of the relationship between the ionic strength and the activity for a solution where the ionic strength is lower than 0.1M.

For higher ionic strength, more sophisticated equations must be used and thus is not convenient to derive this value based on a numerical formula; rather it is preferred to use actual empirical data for calculations involving high ionic strength. Therefore, standard Gibbs free energy of formation data for different biological substances at different ionic strength are measured and catalogued, for the sake of neglecting the term Q in equation (2.2) and (2.3). A table of all relevant substances is listed below in table 2.1 and a complete list can be found in Albety's work [32].

	$\Delta_f G°$/kJ mol^{-1}		
Ionic strength/M	0	0.10	0.25
β -D-Glucose(aq)	-436.42	-429.08	-426.71
δ -Gluconolactone(aq)	-506.38	-500.26	-498.28
H_2O(aq)	-157.28	-156.05	-155.66
O_2(g)	0	0	0

Table 2.1 Standard Gibbs energies of formation $\Delta_f G°$at 25°C, pH 7 [32]

For reaction (1.1) at 25 degrees Celsius, a 0.1 M ionic strength and an oxygen pressure of 1 atm, the EMF is 1.18 V according to equation (2.2) and using data in table 2.1. This value gives the theoretical maximum reversible open circuit voltage based on oxidation of glucose to gluconolactone. In calculation, the assumption is made that no heat is generated, no mechanical friction is included, and no potential loss is considered.

2.1.3. Steady State Behaviour

By applying an external load to a biofuel cell, the equilibrium established is deviated from the original reversible state as calculated above to another irreversible state. The transition from one state to another is observed experimentally and schematically illustrated in figure 2.2.

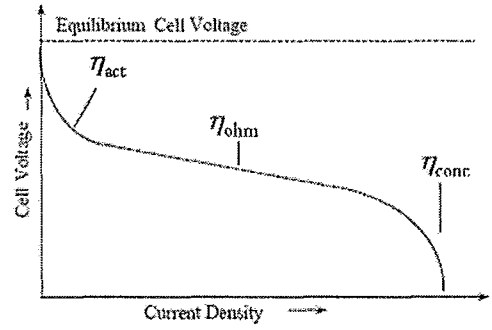

Figure 2.2 Typical voltage/current curve for low temperature/normal atmosphere fuel cell [33]

The curve is categorized by three different overpotentials (a name that comes from electrolysis industry where the minimum voltage applied is always higher than theoretical value). In biofuel cells, overpotentials lower the open circuit voltage but essentially share the same source of irreversibility as observed in electrolysis. Overpotentials are classified according to their source of origin, namely activation, ohmic and concentration overpotential.

Activation overpotential is mainly due to the slow reactions that take place on the surface of electrodes. By forcing the electrons from or to electrodes, a portion of the potential generated is consumed. In figure 2.2, it is the nonlinear portion near y-axis that represents activation overpotential and it reaches its maximum at a certain level before ohmic overpotential's dominate the loss. Ohmic overpotential is caused by resistance that electrons/protons experience as they go through electrode materials and, the interfaces between the different components of the cell. Transportation of the cations in electrolyte also contributes to the ohmic overpotential. This behaviour is represented by the linear part of the graph 2.2, and is the main cause of overpotential

before concentration overpotential causes the rapid drop seen in figure 2.2. At high current density, the portion where the current approaches its maximum, the concentration of the reactants near the active electrode surface depleted by the high reaction rate. This causes the concentration of the reactants to be lower than the average concentration in electrolyte, and gives rise to additional overpotential as governed by Q in equation (2.5).

2.1.4. Transient Behaviour

Thermodynamics is a measure of the equilibrium state even thought it may take a long time to reach. By evaluating the steady state behaviour, we understand that a fuel cell will establish a steady state after a certain incubation period. Transient characteristics of a fuel cell are of paramount importance for real applications. Transient behaviour is the change in current and voltage from the steady state after a sudden switch of external load condition. It is the study of what occurs during the transition from one equilibrium to another. Transient behaviour has been studied by Wang et al. [34] and Um et al. [35] in PEM fuel cells. They believed that for a PEM fuel cell, three primary processes govern the time response. They are (1) electrochemical double-layer (2) gas transport (3) membrane hydration or dehydration. They claimed that the response time of a double-layer is between micro- and milliseconds at a current density of 1A/cm^2, which is sufficiently short to be ignored in real applications. They also claimed that membrane hydration response (from dry to wet) is in the range of 20 to 50 seconds at a current density of 1 A/cm^2. This value is around 15 seconds for a membrane to adjust its own water content on changing the external load.

No detailed discussion has been published regarding biofuel cells because of the multi-disciplinary nature of its mechanism. This process could include time response for membrane hydration, mass transfer of fuel, electrochemical double layer build up and proton/hydroxyl transfer in membrane.

2.2. Overpotential

Literature reviews on electron transfer and overpotentials are listed together in this section. This is because part of the overpotential is caused by electron transfer and it is hard to isolate one from the other. The term overpotential is inherited from electrolysis, a reversed fuel cell reaction. In both electrolysis and fuel cells, overpotentials always impede the output through inner voltage consumption at various interfaces and processes.

2.2.1. Activation Overpotential

Activation overpotential was first observed and then studied by people systematically among the three overpotential behaviours. This highly nonlinear behaviour is caused by slow redox reaction on the electrode surface.

2.2.1.1. Tafel Relation

Tafel in 1905 observed through experimentation that in various electrochemical reactions, the overpotentials of the electrode always followed a similar trend as illustrated in figure 2.3.

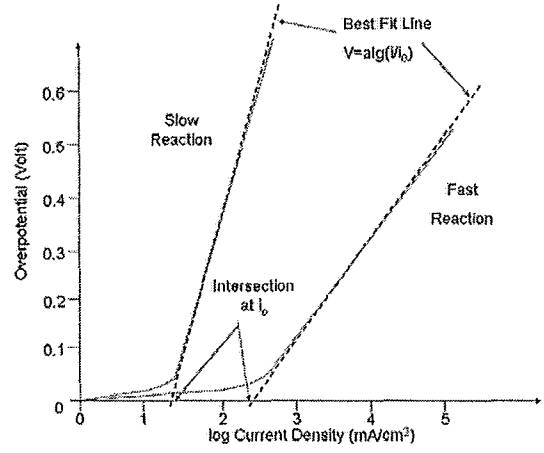

Figure 2.3 Typical Tafel plot for fast/slow reactions

For a current density slightly higher than 0 (it is actually exchange current and will be discussed below), Tafel equation is a good approximation of activation

overpotential in the following form:

$$\Delta V_{act} = A \ln(i/i_0) \quad (2.9)$$

A is a constant that depends on temperature and electrode material; it is different for individual reactions. In (2.9), i is the actual current density of the cell and i_0 is called exchange current. In a fuel cell system, a positive overpotential must always be observed, therefore by mathematically reviewing expression (2.9), Tafel equation is valid only when $i > i_0$. When the overall current density of the fuel cell is 0, we may consider it as being at the equilibrium state, where the forward and reversed reactions are equal. In this case, there is continuous electrons flow in and out of the electrolyte, even if the net current is 0. This continuous equilibrium is called exchange current density i_0 and the higher it is, the more active the surface of electrode. From expression (2.9), we can evaluate that a large value of i_0 and small value of A is preferable when building a fuel cell with low activation overpotential. Unfortunately, i_0 increases with increasing temperature but A decreases with increasing temperature. Fortunately, the effect of rising temperature on i_0 is far more significant than its effect on A. To minimize activation overpotential according to equation (2.9) and figure 2.3, a large i_0 is crucial as it can vary in several orders of magnitude.

In order to maximize i_0, Larminie et al. [33] proposed the following:

1. Increase working temperature of fuel cell. i_0 is a strong function of temperature. An example shown by Wang [36], where i_0 is 0.1mA/cm^2 for a low temperature fuel cell and is 10 mA/cm^2 for the same fuel cell at 800 degrees Celsius.
2. More effective catalyst. It is obvious in figure 2.3 that a faster reaction results in a low overpotential.
3. Increase roughness therefore increase surface area of electrodes and reduced current density.
4. Increase activity of reactants. For instance, using pure oxygen instead of air in a PEM fuel cell.

2.2.1.2. Electrochemical Double Layer

In an electrochemical device, the formation of electrochemical double layer is caused by the diffusion of cations (protons in the PEM and biofuel cells) and anions. As illustrated in figure 2.4, on the cathode of a fuel cell, protons produced at the electrode tend to migrate into electrolyte in order to recombine with electrons transferred from the external circuit. It is obvious that more protons on the electrode surface will increase the possibility of the cathode reaction in equation (2.10).

$$O_2+4e^-+4H^+ \rightarrow 2H_2O \qquad (2.10)$$

An internal potential gradient is therefore formed by this double layer and it gives rise to activation overpotential. The existence of the double layer on electrolyte-electrode interface can be viewed as a charge storage device, a capacitor. When the current changes, charges accumulated on the device will deplete or accumulate.

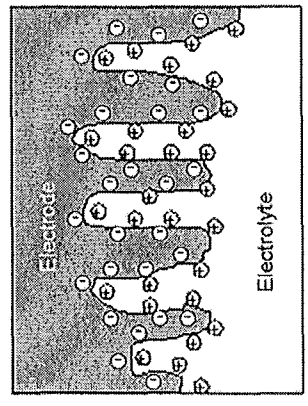

Figure 2.4 Electrochemical double layer

2.2.1.3. Electron Transfer and Efficiency Loss

Membrane and electrolyte are selected as cation transport medium because they can resist the transportation of electrons. This is not always true as a small amount of substrate and electrons can penetrate electrolyte and membrane to cause direct oxidation in the cathode chamber. This direct oxidation reduces Coulombic

efficiency [37]. Coulombic efficiency is the term used to define how much substrate is oxidized through the designated path. In a PEM fuel cell, for each hydrogen molecule or two electrons that penetrate through the membrane to react with oxygen in cathode, two electrons are wasted from an efficiency point of view. Therefore, a short circuit inside a fuel cell from anode to cathode is another cause of activation overpotential even thought it does not take up a significant portion.

2.2.2. Ohmic Overpotential

Ohmic losses in the electrode or ionic transport through the electrolyte give rise to resistance in the circuit, and are the origin of ohmic overpotential. The magnitude of ohmic overpotential is proportional to current density in equation (2.11).

$$V_{ohm}=ir \tag{2.11}$$

Part of this loss is caused by the transportation of electrons in the external circuit, as illustrated by the linear portion in figure 2.2. The power is released by the fuel cell as dissipated heat.

2.2.3. Concentration Overpotential

Concentration overpotential is valid only when the current density is relatively high and it is highly nonlinear according to figure 2.2. In a PEM fuel cell, for instance, hydrogen is pumped into anode. The direct result of high current density is a high rate of consumption of hydrogen, which results in a decrease in hydrogen concentration near the electrode surface. In the case of a biofuel cell, concentration overpotential results from the concentration of protons near the electrode being relatively lower than the concentration of the bulk electrolyte. It is a result of rapid proton migration through the membrane to cathode. Schematically in figure 2.5, the concentration profile of the active ion (the proton in PEM cells and biofuel cells) along the electrode interface generates a diffusion layer between the bulk solution and the electrode.

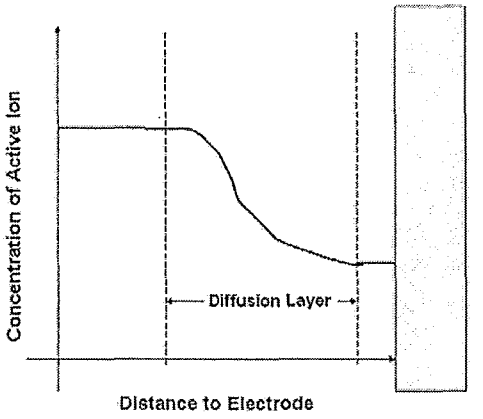

Figure 2.5 Concentration profile near electrode surface

More precisely, concentration overpotential is the difference in potential between an electrode with the lower interfacial concentrations and the potential the same reference electrode with the interfacial concentration of the bulk solution [38].

By using the Nernst equation, the loss in potential of a PEM fuel cell due to a change of gas pressure is as follows:

$$V = (RT/nF)\, ln(P_2/P_1) \tag{2.12}$$

Where P_1 is the theoretical maximum rate of gas supply and P_2 is the true gas supply. By assuming an extreme current density i_1, which is the current generated at P_1, the pressure at any value can be written as:

$$P_2 = P_1(1-i/i_1) \tag{2.13}$$

By combining with equation (2.12),

$$V_{con} = (RT/nF)\, ln(1-i/i_1) \tag{2.14}$$

Another relation based on experimental results is also a good estimation of the concentration overpotential and is widely used by researchers [39]:

$$V_{con} = m\, exp(ni) \tag{2.15}$$

By carefully selecting m and n, expressions (2.14) and (2.15) are highly consistent with each other. Electron transfer is rapid, and therefore does not result in concentration overpotential.

2.2.4. Summary of Overpotential

The total overall effect of overpotentials can be written as:

$$V = E - \Delta V_{act} - \Delta V_{ohm} - \Delta V_{con} \quad (2.16)$$

$$V = E - A\ln(i/i_0) - ir - m\exp(ni) \quad (2.17)$$

Tsujimura et al. in 2002 [40] proved that this behaviour was also correct in a glucose/oxygen biofuel cell in figure 2.6

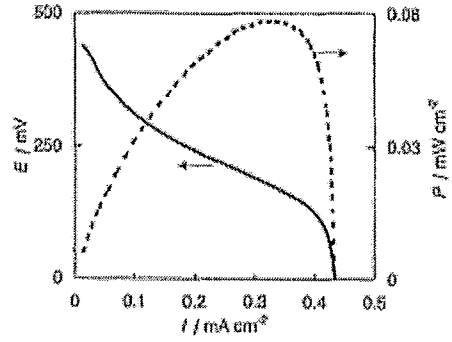

Figure 2.6 Performance of a glucose/O_2 biofuel cell [40]

The overpotential is a function of current density and only starts when current density i exceeds the exchange current i_0 in the circuit. Electron transfer is responsible for part of activation overpotential and the majority of ohmic overpotential.

2.3. Proton Transport and pH Gradient for Low Power Density

2.3.1. Protons' Driving Force in Nafion

In the well studied PEM fuel cell, hydrogen gas disassociates into protons, which then migrate freely into the membrane and subsequently towards the cathode. This dissociation (2.18) occurs spontaneously because of the equilibrium ratio of hydrogen ions and hydrogen molecules at a given temperature.

$$H_2 \rightarrow 2H^+ + 2e^- \quad (2.18)$$

The existence of platinum as catalyst on the anode helps to speed up this process. The driving force which pushes the first proton towards cathode via membrane is the difference in chemical potential. By definition, the chemical

potentials of protons are the same at both the anode and the cathode at equilibrium as shown in equation (2.19). The superscript *a* and *c* denotes the anode and the cathode.

$$\mu^a(H^+)=\mu^c(H^+) \quad (2.19)$$

As positively charged protons move towards the cathode, the difference in the chemical potentials of the protons at the anode and protons at the cathode becomes smaller. As a result, the excess electrons on the electrode create a negatively charged anode and therefore form a double layer as described in 2.2.1.2. Furthermore, electrons in the negatively charged anode tend to move to the positively charged cathode through the external circuit. The cathode is positively charged because the electrons recombine with oxygen gas and protons through a mechanism described by the bridge model as illustrated by Yeager et al. [41] in figure 2.7. The model essentially describes the role of platinum during combination of oxygen gas and proton to form water.

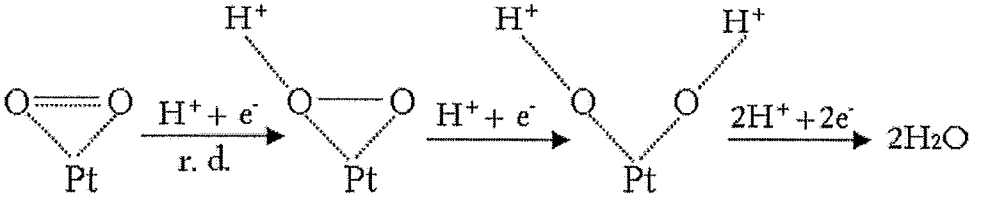

Figure 2.7 The Bridge model of oxygen reduction [41]

2.3.2. Modes of Proton Transfer in Membrane

The previous section discussed the motion of protons before and after passing through the membrane. For the purpose of understanding the membrane properties it is useful to use the well-studied Nafion membrane basis. Nafion dominates PEM fuel cell applications and it is also largely used in biofuel cells.

2.3.2.1. Introduction to Nafion

Nafion is a sulfonated tetrafluorethylene polymer, as illustrated in figure 2.8. Nafion possess unique hydrophobic and hydrophilic properties. Tetrafluorethylene, or

Teflon, is known as a hydrophobic material, however the sulfonate groups attached to the end of carbon chains in the Nafion structure tend to adsorb water molecules. Each sulfonate can grasp one proton for approximately every 20 water molecules absorbed on the surface, in a well-hydrated situation. Nafion therefore behaves as an acidic membrane when soaked in water. By moving protons from one sulfonate to another, a stream of positively charged cations can be transported through the Nafion membrane.

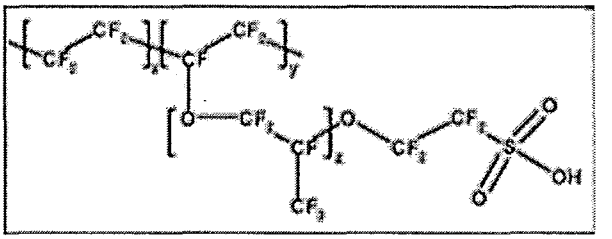

Figure 2.8 Structure of Nafion [42]

Nafion, which only conducts cations, is widely used in hydrogen PEM fuel cells because protons are the only cation in the system.

For the construction of a complete biofuel cell, it is mandatory to couple the anode and the cathode units. The proton exchange membrane, such as Nafion is extensively used not only because it can theoretically conduct protons, but also because it prevents the direct oxidation of the fuel. In conventional fuel cells, as discussed in 2.2.1.4, a part of activation overpotential is the result of fuel penetration. This results in a significant voltage loss in the case of methanol fuel cells. Similarly in a glucose/oxygen biofuel cell, if the cell is not sealed properly between the anode and the cathode, glucose dissolved in buffer can diffuse to the cathode and react directly with oxygen.

2.3.2.2. Transport Mode

Streams of cations flow in the electrolyte completing the internal circuit as long as the external electrical circuit is complete. In a transient study of a Nafion membrane, a revised form of the Nernst-Plank equation is used. Nernst-Plank equation is used to describe a flux of ions through a diffusive membrane under the

influence of both an ionic concentration gradient (C) and an electric potential (Φ) in (2.20). D_i is Diffusivity of species i (cm^2/s), C_i is the concentration of species i (mol/cm^3); and x is distance (m) in the direction of diffusion.

$$J_i = -D_i \frac{dC_i}{dx} - D_i \frac{z_i C_i F}{RT} \frac{d\Phi}{dx} \tag{2.20}$$

It is clear that the first term is an expression of Fick's first law and represents diffusion. The second term in (2.20) denotes migration.

$$J_i = -D_i \frac{dC_i}{dx} - D_i \frac{z_i C_i F}{RT} \frac{d\Phi}{dx} + v_k C_i \tag{2.21}$$

Furthermore, Strathmann et al. [43] expanded this equation into equation (2.21) by adding a convection term $v_k C_i$. An internally generated electrical potential causes diffusion; the electrochemical reaction itself causes migration and diffusion of water resulting in a convectional proton flux.

2.3.2.3. Water Content and Proton Hindrance

As explained in the last section, water in Nafion permits the movement of protons from their original site to an adjacent one. Both experimentation and theory show a highly consistent conclusion that Nafion is not conductive in its dry form. However, for Nafion, being immersed in solution is not sufficient to maintain necessary hydration. Researchers have also found unexpected contamination due to cations that take the place of the designated proton positions in the PEM fuel cells. J. St-Pierre et al. in 2000 [44] proposed that larger cations penetrating into the Nafion attenuated the electric conductivity by decreasing the number of water molecules around each sulfonate group. Larger cations penetrating into the Nafion lowers the transportation coefficient of water molecules in Nafion. This behaviour increases the internal resistance of the fuel cell even when the large ions are in very low concentration (contamination level, 10^{-5}-10^{-6} mol/L). A direct consequence of larger cations contaminating the Nafion is the accumulation of the protons produced by

oxidation at the anode. As a result a pH drop is expected and has been observed in St-Pierre's paper followed by degradation of the fuel cell output. It has been concluded for a PEM fuel cell that water management as well as control of large cation impurity is crucial from the engineering prospective.

2.3.2.4. pH, Proton and other Ions in Electrolyte

Glucose/oxygen enzymatic fuel cells depend solely on protons and electrons provided by the oxidation of glucose at the anode. As a result, the activity and stability of the enzyme has to be accounted for in order to determine the cell performance. Activity data of glucose oxidase (GOx) taken from Roche Applied Science as shown in figure 2.9 indicates that the relative activity of the enzyme is severely influenced by acidity of its environment. The graph shows that the performance of GOx is stable when the pH ranges from 5 to 7 and becomes highly inactive in even slightly basic solution.

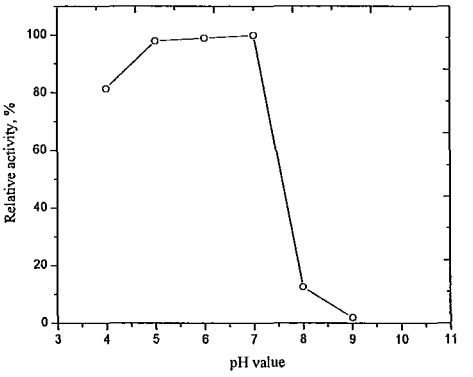

Figure 2.9 pH and glucose oxidase activity

Therefore, phosphate buffer solution is often used to adjust the proton concentration of electrolyte in enzymatic biofuel cells. It has been proven by Jang et al. [15] that even when salts such as a phosphate buffer solution are used in the anode half cell, proton transport through the membrane is inhibited. It was concluded that there was still the need for the efficient diffusion of protons through the aqueous phase by enhancing the ionic strength. Therefore, when a liquid phase electrolyte is

used, low buffer concentration does harm to the physiological condition, and also kills proton migration at the anode. By introducing phosphate buffer solution, large cations such as potassium or sodium are inevitably brought in to the Nafion membrane. No significant difference was observed based on if the cation was sodium or potassium (sodium is used in our experiment). The existence of sodium makes an enzymatic fuel cell a more complicated system than PEM fuel cells. In order to be an effective buffer solution, the concentration ratio of Na^+ to H^+ should be sufficiently high, 10^6 is a reasonable approximation.

2.3.2.5. Problem Observation and Discussion

The topic of proton transportation and pH deviation in microbial fuel cells was first focused on in 2003 by Gil et al. [45]. A decrease in pH at the anode and an increase in pH at the cathode were observed during operation of a two-chamber microbial fuel cell. Rozendal et al. [46] in 2006 discussed that within a microbial biofuel cell system, the cations responsible for the penetration from anode to cathode were potassium, sodium, magnesium, and not the previously proposed protons. As a result, these large species accumulate in the Nafion membrane and increase the resistivity of membrane. Consequently, accumulated cations at the anode replace the protons that are supposed to be oxidized to water in the cathode. Instead, water molecules react with electrons from the external circuit to form OH^- to maintain electroneutrality. In addition, the concentrations of other cation species in the anolyte are significantly higher than the concentration of the protons, thus proton transport is negligible. Analysis of the membrane taken from a microbial fuel cell used in Rozendal's setup shows that K^+ and Na^+ take up 74% of the sulfonate residue.

The above discussions and arguments explain the observation of Gil et al. [45] and Liu and Logan's [47]; lowering of cathode potentials is caused by alkalization in the cathode compartment.

Furthermore, in 2008 Chae et al. [47] confirmed this result using X-ray (EDX)

analysis. Chae et al. showed that the relative atomic percentage of carbon (30.9%) and fluoride (59.7%), the basic backbone materials of Nafion, has been lowered in a piece of used Nafion, as compared to a piece of new Nafion (C=32.8%, F=60.1%). At the same time, sodium and iron, ions that do not exist in Nafion, increases by 1.16% and 0.24%. They concluded that these cations cause the hindrance of proton transportation.

Additionally, Kim et al. in 2007 [22] believed that with the presence of phosphate buffer at the anode, no protons were able to penetrate the membrane. All electricity generated during operation of the cells, was due to either the oxidation of pre-treated protons in the Nafion or from the reduction reaction (2.22) at the cathode:

$$4e^- + 2H_2O + O_2 \rightarrow 4OH^- \qquad (2.22)$$

Kim's result is highly consistent with the concern expressed by Gil et al. [45] on pH increase at the cathode. As long as protons are hindered, there is not sufficient proton transportation to recombine with the surplus electrons and oxygen gas. Reaction (2.22) appears to be an alternative, but this reaction is only operative at the beginning of the experiment. Hydroxyl accumulation in cathode will in turn prevent the reaction from proceeding in the forward direction any further. Therefore the larger the pH deviation in anode and cathode chambers, the lower the power output of the microbial fuel cell.

We are now able to realize the conflict between sodium ions and protons in this process. In a microbial fuel cell, high concentration of sodium from the buffer solution impedes similarly the effective transport of protons. Sodium ions and protons serve the same purpose, however the two cannot coexist peacefully in the Nafion. The dilemma between buffer solution and membrane properties has become the source of a bottleneck in biofuel cell research and this conclusion has been confirmed by all researchers who are mentioned above in section 2.3.2.5.

2.3.2.6. Problem Confirmation in Enzymatic Biofuel Cells

All discussions in 2.3.2.5 are based on the microbial fuel cell, but this does not constrain the validity of the problem of low power density from application to enzymatic biofuel cells. All physical parts in 2.3.2.5 in a microbial fuel cell have their equivalent counterparts in an enzymatic biofuel cell. To verify if we are able to extend the problem discussed above to an enzymatic biofuel cell, a range of experiments are to be conducted. The detailed experimental procedures will be discussed in the next chapter.

It has been found that similar pH drop and consequential drop in power output with respect to time can be observed for both types of biofuel cells. Figure 4.1 and 4.2 which confirm that the problem is applicable to both types of cells can be found in chapter 4.

2.4. Survey of Possible Solutions

Individual discussions about the buffer and the membrane in microbial fuel cells have been published only recently and will be introduced in this section in greater detail. No paper up to now, to our knowledge has systematically solved the dilemma pertaining to membrane properties and electrolyte acidity. In this section, a series of solutions will be proposed followed by possibilities for application and any, related research from other authors. The dilemma is resolved if any of the two elements (buffer and membrane) is removed, this is feasible provided an alternative is introduced to maintain their original function without the addition of any new unwanted problems. According to this logic, four possibilities are discussed in sequence.

2.4.1. Selective Membrane

Among the two elements in the dilemma, the use of a membrane appears to be

the easiest to tackle. The use of Nafion in a biofuel cell stems from PEM fuel cells where protons are the only cations present in the system. The membrane is used to isolate the anode and the cathode by its unique partial hydrophobic and partial hydrophilic properties. It is not adequate to adopt Nafion as an ideal membrane material in biofuel cells with sophisticated biological reactions. If we want to adopt the use of a phosphate buffer solution, a membrane that only conducts protons is necessary. Unfortunately, no such membrane has ever been discovered or synthesized. It has been proposed that biological selective membranes could be a possible solution but require further research. Biological selective membranes, such as cell membranes, are semipermeable membranes that selectively permit the penetration of some molecules in spite of their sizes. This selective property is related to the membranes biological function and it has never been mentioned in biofuel cells research. The search for biological selective membrane remains a future direction for biochemists.

2.4.2. Membraneless Structure

Another idea which relies on the membrane is to remove the need for the membrane by making the bioelectrocatalytic reaction indifferent to the interfering components. Katz et al. in 2003 [48] reported a glucose/oxygen fuel cell, using PQQ-FAD/GOx and Cytochrome c/Cytochrome oxidase. The oxidases mentioned were all functionalized on Au-electrodes as catalysts for the anode and the cathode respectively. In this case, glucose is unaffected by oxygen because of the efficient bioreaction between glucose and the modified enzymes.

Liu et al. [37] did a systematic comparison of an air-cathode single chamber microbial fuel cell in the presence and absence of Nafion. In the case without a membrane, the catalyst must be immobilized onto the electrode surface. This complicates the fabrication process of the fuel cell. They found that by removing the membrane there was an increase in the power density by 88.5 % and this was attributed to an increase in the open circuit voltage. They proposed that, by removing

the Nafion membrane, it was likely that the internal resistance of the system was reduced and lead to less resistance for the proton transfer from the anode to the cathode. On the other hand, they also found that, without a membrane, the Coulombic efficiency was only 9%-12%. The typical value for a membrane system is 40%-55%. This illustrates another pertinent issue for membraneless system: oxygen diffusion. The most likely reason for a low Coulombic efficiency is the loss of substrate/fuel due to diffusion of oxygen from the cathode to the anode. Oxygen diffusion through the Nafion membrane at a rate of 0.05 mg/min can account for an aerobic loss of 28% of the glucose added, when the concentration is 600mg/L and after the cell has been operated for 100 hours. If the loss of substrate to oxygen is accounted for, the remaining portion of electrons based on Coulombic efficiency calculation is reduced from 45% to only 17%.

Some recent papers with membraneless structure either put emphasis on wastewater treatment or on the miniaturization of the structure. Commercially available Nafion is about $100 US per square meter. For wastewater treatment biofuel cells, high power density is not as important as the scale of the cell and the price of materials used. Biofuel cells of large size, which are constructed of cheap materials, and have very low power output, have been reported [49] [50]. On the other hand, it is hard to achieve an ideally sealed compartment for miniature cells since the electrodes used are micrometers in diameter. Chen et al. [51] reported a miniature biofuel cell using glucose/GOx with a maximum power density of 0.13mW/cm^2. They wired GOx and a mediator onto the anode on a polymer substrate in a sophisticated way. Phase-separation of GOx from the wiring polymer is prevented by electro-static coupling of the polycationic wires and the enzymes. Selective oxidation enzymes are also immobilized on the cathode. Therefore, the roles of cathode and anode are decided by the selective nature of the enzymes wired on each electrode. In 2008 Call et al. [53] reported a novel membraneless electrohydrogenesis system.

Electrohydrogenesis is an electrolysis method for directly converting biodegradable material into hydrogen gas using a modified microbial fuel cell. He concluded that the system without a membrane can potentially affect the purity of the gas produced.

To summarize, membraneless structured biofuel cells have either low Coulombic efficiency or high materials cost due to the sophisticated immobilization techniques used in the construction. It is therefore not an ideal solution to the dilemma of membrane and electrolyte properties.

2.4.3. Tris Buffer

The last two solutions focused on the membrane component instead of the buffer solution. An alternative buffer solution that can provide an appropriate environment for living enzymes could be another solution to the problem.

$TrisH^+$/Tris buffer is one of the common biological buffers which do not contain any alkali or alkaline earth metal ions. It can provide a neutral pH solution and has a structure as illustrated in figure 2.10.

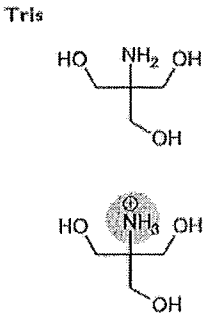

Figure 2.10 Structure of $TrisH^+$/Tris buffer [52]

It is proposed that the use of $TrisH^+$/Tris buffer will cause a smaller pH gradient between the anode and the cathode due to the nature of the cation. An experiment to test this hypothesis will be conducted in next chapter.

2.4.4. Anion Exchange Membrane

2.4.4.1. Mechanism

A biofuel cell system utilizing cation exchange membrane (CEM) such as Nafion follows the behaviour described by equation (1.1), (1.2) and (1.3). Essentially equation (1.3) is the governing equation, where as equations (1.1) and (1.2) are half reactions which only describe the molecule separation and recombination at the anode and the cathode. An anion exchange membrane (AEM), if properly used, follows equation (1.3) by isolating the recombination of protons and electrons at the anode instead of at the cathode. Equation (2.23) and (2.24) are half reactions proposed in an anion exchange membrane based biofuel cell.

Anode: 2β - D-glucose $\rightarrow$ 2δ – gluconolactone + $4e^- + 4H^+$ (2.23)

Cathode: $4H^+ + 4OH^- \rightarrow 4H_2O$

$H_2O + O_2 + 4e^- \rightarrow 4OH^-$ (2.24)

Overall, if we add equation (2.23) and (2.24), we have the same resulting equation (1.3).

2.4.4.2. Literature on AEM

In 2007 Rozendal et al. published the first paper involving an AEM biofuel cell [55] and was followed by another publication in 2008 [54]. Both papers are based on the electrohydrogenesis system. In these two papers, Rozendal et al. concluded that AEM are better than CEM in terms of the ability to prevent the formation of a large pH gradient across the anode and the cathode. However, an AEM caused a higher overpotential in the cathode than a CEM. Another group has done similar work in the recent years. Their first paper involved the comparison of different membranes in a microbial biofuel cell system and was published in 2007 [56]. It was concluded that AEMs showed the highest Coulombic efficiency and power output among all candidate membranes including Nafion, and other CEMs. A year later in 2008, another researcher, Cheng [57], belonging to Rozendal's group concluded that for his

electrohydrogenesis system at an applied voltage higher than 600mV, the hydrogen production rate continued to increase using an AEM but not for a CEM. He also discovered that AEM system produced a smaller pH gradient across the membrane than CEM system. Concurrently in 2008, another researcher Zuo [58] in this group studied the behaviour and performance of AEM in microbial fuel cells for wastewater treatment. He found that, by using a cheap AEM and nonprecious metal catalyst, the system provided comparable performance to a similar system which used materials costing nearly an order of magnitude more. Thus AEMs represent more useful materials for reducing the cost of microbial fuel cells for wastewater treatment.

The works above were all based on a microbial biofuel cell system; independent of whether they were used for waste water treatment or electrohydrogenesis. No systematic study has been done for an enzymatic biofuel cell, which is slightly different than a microbial system. Making the anode and the cathode pH close to each other and achieving a relatively high power density are the two main objectives in the search of appropriate membrane material.

2.5. PEM Internal Circuit and Transient Measurement

2.5.1. Equivalent Circuit

As explained in section 2.2.1.3, a double layer is the cause of activation overpotential. An electrochemical double layer near or on the electrode-electrolyte interface is considered the same as a device for charge and energy storage. A capacitor made of a layer of dielectric material sandwiched by two pieces of conductive materials in electrical circuit similarly plays the role of charge and energy storage. In a PEM system the anode electrode is composed of nanometer-scale platinum particles, acting as catalyst bonded to the carbon particles which make up the bulk of the electrode as seen in figure 2.11.

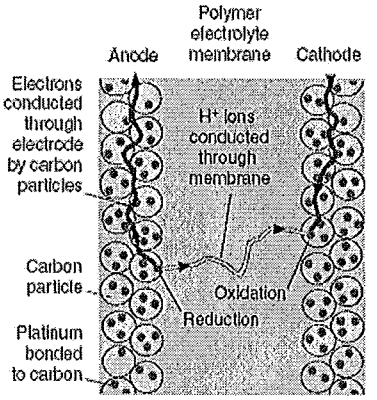

Figure 2.11 Electrode structure of PEM fuel cells [53]

The triple-phase area of gas/platinum/carbon particle is essentially where the anodic double layer is formed for a PEM fuel cell. Once the hydrogen gas is split by the platinum into protons and electrons, the protons tend to stay on the outer surface of the carbon particle near the Nafion membrane. This trend is caused by the chemical potential difference. However, electrons can only stay inside conductive carbon particles. Therefore, a large number of mini-electrochemical double layers are formed. The overall capacitance effect is essentially the sum of all of the mini capacitors (as if all are connected in parallel). An equivalent circuit is drawn in figure 2.12 based on the assumptions and observations in section 2.2 and 2.5.

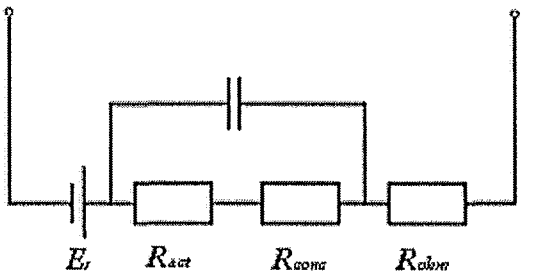

Figure 2.12 An equivalent circuit model of a PEM fuel cell [33]

A resistor R_{act} and a capacitor placed in parallel simulate the voltage loss due to activation overpotential. Another resistor R_{conc} represents the loss caused by the concentration overpotential and it is often neglected in biofuel cells due to their relatively low current density.

A resistor R_{ohm} is in series with the activation overpotential components, and represents all ohmic loss inside a fuel cell. Generally speaking, the presence of the capacitor in the equivalent circuit makes the fuel cell perform well in terms of kinetics. More specifically, the voltage and current smoothly move from one value to another as the external load changes.

2.5.2. Transient Measurement

2.5.2.1. Current Interruption

Overpotentials caused by different mechanisms can not be separated using any steady state measurement technique. This is because all of the overpotentials are thermodynamically decided and can be viewed as a whole in a steady state study. Current interruption, however, is a simple and quick method to precisely distinguish ohmic resistance from the activation resistance. The principle method employed in this technique is to use a very fast switch to momentarily open-circuit the cell and then to measure the cell voltage immediately after this interruption.

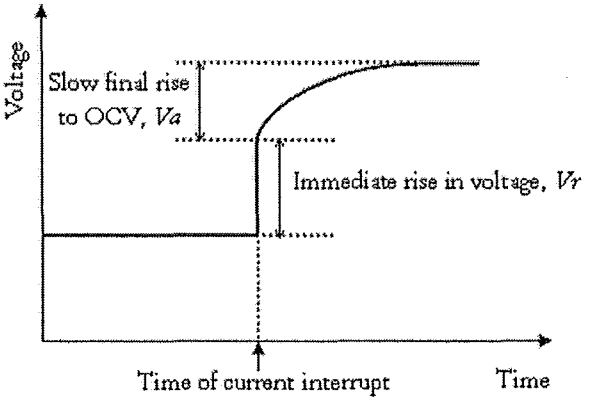

Figure 2.13 Schematic illustration of voltage vs. time plot during a current interruption experiment

When a fuel cell is working at a given external load, the voltage and current density will become stable after its initialization. The voltage deviates from its open circuit voltage because of the presence of activation overpotential and ohmic overpotential. If the load is removed, the voltage will go back to its open circuit

voltage eventually. Ohmic overpotential disappears almost instantaneously, whereas the relaxation time of activation overpotential is significantly longer. Losses due to ohmic effect *Vr* and losses caused by electrochemical double layer *Va* constitute the difference between open circuit voltage and real output voltage before switch. The behaviour of the voltage and current before and after interruption is schematically drawn in figure 2.13. This technique has been used extensively in PEM fuel cell, solid oxide fuel cell and direct methanol fuel cell research. It is concluded that for a low temperature PEM fuel cell at a medium current density ($100mA/cm^2$), activation overpotential and ohmic overpotential are relatively of the same magnitude [33].

2.5.2.2. Load Step Measurement

Load step changes in the external resistance are produced using an in-house designed resistance board with short switching time. This consists of a parallel combination of two resistors. A circuit diagram of the experimental set-up is shown in figure 2.14. When R_2 is disconnected, the total external resistance switches from the paralleled combination of R_1 and R_2 to R_1 only. By applying this dynamic behaviour to biofuel cells, we are able to investigate how fast biofuel cells respond to load change under fixed properties such as temperature.

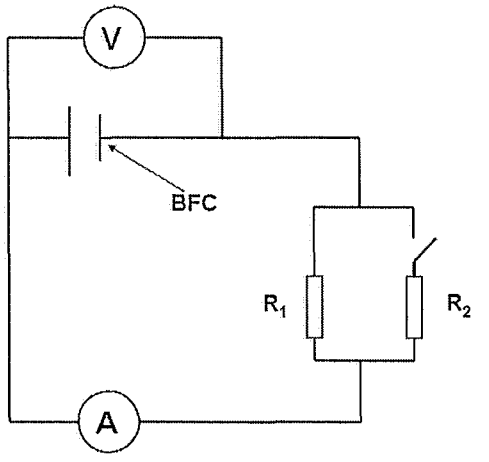

Figure 2.14 Set-up for load switch test

To the best of our knowledge, load step measurement and current interruption

method have not been employed in the study of enzymatic biofuel cells to date.

3. Experimental Setup

3.1. Biofuel Cell Design and Construction

As shown in figure 3.1, the biofuel cell setup used in these experiments is a two chamber structure with a conventional platinum-based cathode and bio-anode. The anode and the cathode compartments are separated by a half Membrane-Electrode-Assembly (MEA) made of a semipermeable membrane and a piece of carbon cloth.

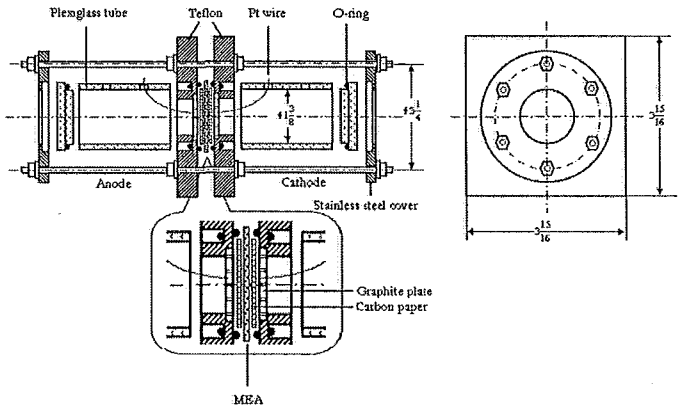

Figure 3.1 Schematic Diagram of our biofuel cell

The Anode and cathode chambers made of plexiglass and fit into two ports located on the MEA. Two graphite plates (Speer Canada Inc., Canada) with 21× Φ2 mm holes are placed between two chambers. These graphite plates, with surface area of 6.2 cm^2, serve as the electrode in the anode and the current collector in the cathode. Copper wire (Arcor Inc, USA) attached to the electrode passing through the chamber is connected to the external circuit. Two O-rings on plexiglass covers and four O-rings on Teflon plates provide a tight seal for the anode chamber. The MEA is sandwiched between two Teflon plates and fastened by 12 bolts, washers and nuts. The plexiglass tubes are sandwiched to the Teflon plates and fastened by 6 bolts, nuts

and washers. We have hereby proposed a system with electrolyte seal and good electrical contact.

3.2. Buffer, Fuel, Mediator, Enzyme and Electrolyte Preparation

The Glucose Oxidase (GOx) used in this experiment was purchased from Sigma-Aldrich, Canada is in activity of 216 units/mg. (Biochemically, 1U corresponds to the amount of enzyme that oxidizes 1 μ mol glucose per min at pH = 7.0 and 25℃).

Phosphate buffer solution (0.1 M, measured pH 7.23) was made from Na_2HPO_4 and NaH_2PO_4, and was purchased from Sigma-Aldrich, Canada.

Tris buffer solution (0.1 M, measured pH 7.20) was made from Tris, purchased from Sigma-Aldrich, Canada.

The β-d-glucose solution in the phosphate buffer was allowed to mutarotate for 24 h before use and it was purchased from Sigma-Aldrich, Canada.

Ferrocene Monocarboxylic Acid (FMCA) was chosen as mediator because of its ability to aid electron transfer and has an appropriate redox potential relative to glucose. It was purchased from Sigma-Aldrich, Canada. The structure is graphed below in figure 3.2 and according to Pandey et al. [24], Fe molecule is the atom that accepts and donates the electron during transport of the electron from the substrate to the electrode.

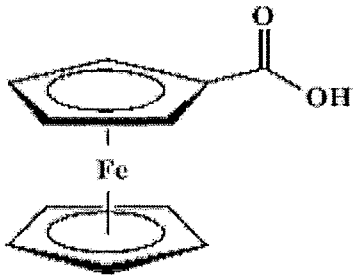

Figure 3.2 Molecular Structure of Ferrocene monocarboxylic acid (FMCA) [24]

Carbon Cloth (E-Tek Inc., USA) was washed by Deionized (DI) water before

each test. A 1.0 mg/cm^2 loading of Pt was immobilized on the carbon cloth.

All solutions were prepared using DI water and solids were completely dissolved using an Ultrasonic Cleaners, Model 1510 (Branson Inc., USA).

3.3. Membranes and Their Pretreatment Procedures

Nafion 117 purchased from DuPont, was pretreated with a standard cleaning procedure: (i)boiling in 3% hydrogen peroxide for 1 h to oxidize organic impurities; (ii)rinsing with boiling water for several hours; (iii)boiling in 1M sulfuric acid for 1h to remove any metallic/ionic impurities; and (iv)rinsing again in boiling water to remove any excess acid.

AMI-7001 (AEM) was purchased from Membranes International Inc., USA.

Fumasep (AEM) was purchased from FuMa-Tech, Germany.

EXCELLION I-100 (AEM) was purchased from Snowpure, USA.

All AEM are stored in DI water expect for AIM-7001 which was stored in 0.1 M phosphate buffer solution.

3.4. Experimental Set-up

Figure 3.2 shows the experiment setup for the biofuel cell operation and measurement apparatus. Nitrogen gas is pumped into the anode chamber for the sake of providing an anoxic environment and a homogenous fuel/enzyme concentration. Air or oxygen is pumped in to the cathode chamber to provide adequate oxidation gas at a constant rate. If not specified, Nitrogen and air are used at a constant rate of 10 ml/min for all experiments. A temperature controlled water bath is used to maintain different experimental temperatures. A pH meter is used to monitor the pH value in the anode compartment. Experimental data acquisition was controlled by general purpose interface bus (GPIB) interface, along with programs written in Quick Basic, and data was recorded to a personal computer.

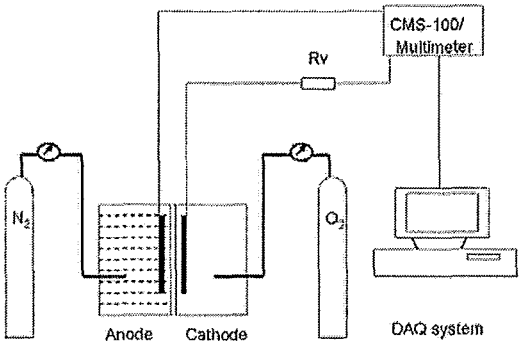

Figure 3.3 Schematic of our biofuel cell's operation and measurement apparatus

3.5. IV Measurement

Cell current and voltage are measured using HP 3478A multimeter (Electrolab Inc., USA) from open circuit to a small external load. The biofuel cell was allowed to equilibrate at open circuit for 1 hour until has stabilized. A five minutes interval relaxation time is allowed between every resistor measurement. The power density is calculated using equation (3.1) based on an effective area of 6.2 cm^2.

$$P = V_{cell} \times I_{cell} \tag{3.1}$$

3.6. Transient Current Measurement

By changing external loadings, the relaxation time for a biofuel cell caused by electrochemical double layers can be measured, this is assumed to be larger than the instantaneous ohmic change. CMS 100 Corrosion Measurement System (Gamry Instruments Inc., USA) is used to monitor transient current change. It also provides us with the possibility to apply an external current and therefore perturb the current generated by the biofuel cell. By interpreting the magnitude of the relaxation time, it may be possible to elucidate information on internal circuit. A proposed equivalent circuit for a PEM fuel cell is given in figure 2.16.

3.7. pH Measurement

The pH values of the electrolyte are measured using ExStik pH 110 meter (Extech Instrument Corporation, USA) which was calibrated carefully before each measurement.

3.8. Impedance Measurement

Internal resistances of all membranes were measured using Parstat 2273 advanced electrochemical system (Princeton Applied Research, USA). The R-X mode of measuring the real and imaginary part of the complex impedance was chosen. Twenty frequencies ranging from 20 Hz to 100 KHz were employed for each series of measurements. The principle of this method is the application of a small sinusoidal perturbation in the potential at different frequencies to the test element. The response is an alternating current signal of the same frequency with a phase shift and change in amplitude. The AC response of the fuel cell can provide additional information on the investigated system.

4. Results and Discussion

4.1. Alternatives to the Problem of pH Gradient

Chapter 3 gives a brief overview of recent research with respect to the problem of low power density. Since the discovery of the problem of low power density in biofuel cells, people have realized that power density is hindered by the reduction in transportation of protons across the membrane, and by the establishment of a pH gradient. By eliminating two unfeasible alternatives to this problem in the literature survey, the two remaining solutions are to be investigated via series of experiments.

According to the result from Zhi's master thesis [60] in 2006, the optimized concentration of glucose, GOx and FMCA in our enzymatic biofuel cells are 200 mmol/L, 0.6 g (based on 50 mL of electrolyte) and 4 mmol/L respectively. This combination of all substances as well as 0.1 mol/L phosphate buffer is adopted in the anode because it should produce the highest current density and power density. A higher power output signal is ideal for calculations and discussions as it maximizes the signal/noise ratio.

4.1.1. Problem Confirmation

As discussed in chapter 2, all literature currently published on the topic of pH gradient across a membrane are based on microbial fuel cells. Figure 4.1 and 4.2 schematically confirmed a similar phenomenon in a glucose/oxygen enzymatic biofuel cell.

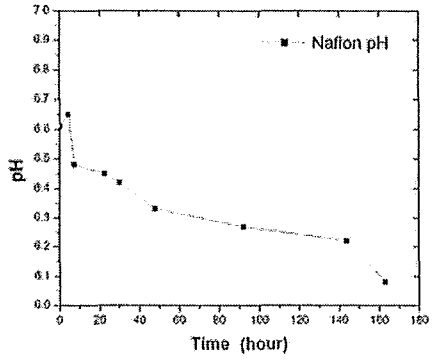

Figure 4.1 pH in a Nafion based enzymatic fuel cell and time

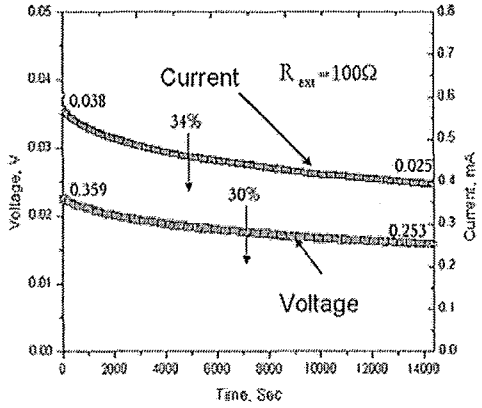

Figure 4.2 Current, power output and time in a Nafion based enzymatic fuel cell

4.1.2. Tris Buffer Alternative

Tris/TrisH^+ buffer as anolyte substrate solution was first tested under physiological conditions. The goal of this experiment was to compare a Tris buffer with a phosphate buffer solution with the same ionic strength. Even thought ionic strength is a function of the number of charges on the cations and concentrations of the species as described in chapter 2, the two ionic strengths were similar in magnitude so long as a dilute solution of similar concentration was used. Therefore a 0.1 mol/L Tris buffer was adopted. After being ultrasonically stirred at room temperature for sufficiently long, the residual of undissolved FMCA was found on the surface of buffer solution despite the fact that this amount of FMCA can be easily dissolve in an equivalent phosphate buffer solution at the same temperature.

The performance test of Tris buffer based biofuel cells was conducted using Nafion as the membrane. A plot of pH as a function time (figure 4.3) was plotted while an external load was connected to the biofuel cell. The first point at time zero was measured right after GOx was added to the solution.

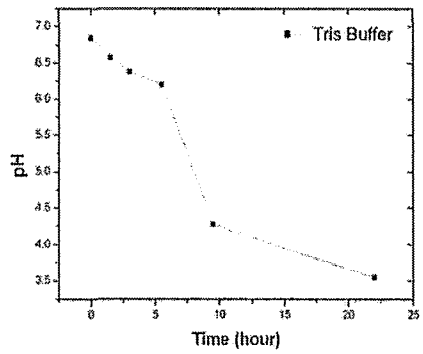

Figure 4.3 pH in a Tris buffer based biofuel cell and time

It is obvious from figure 4.3 that the expected pH stabilization has not been achieved. Comparing the above results with the pH - time behaviour of our phosphate based biofuel cell (figure 4.1), the Tris solution shows more severe pH decay. The experiment of Tris buffer based biofuel cells was halted before 180 hours because it showed no sign that it can accommodate the pH gradient across the membrane.

In our proposed mechanism for Tris buffer based biofuel cells, the cation NH_3^+ has next to none interaction with protons produced by glucose in terms of proton transportation in the Nafion membrane. In the anloyte, proton accumulation caused by the biological oxidation reaction has the tendency to decrease the pH. $CNH_2(OH)_3$ groups can absorb protons to form $CNH_3(OH)_3^+$, so that the influence of increasing acidity is reduced. The Tris buffer solution would work well in other systems with an optimal pH of between 7 to 9 according to the mechanism proposed above.

In summary, Tris/TrisH^+ buffer is not an ideal alternative to a phosphate buffer that can potentially solve the problem of the pH gradient across the membrane.

At the same time, it still remains a challenge to future researches to develop other organic buffer solutions. It will remain inconclusive that phosphate buffers are optimal for this application, until exhausting all other appropriate organic buffers.

4.1.3. Anion Exchange Membrane

In Zhi's [60] work on glucose/oxygen biofuel cells, a Membrane-Electrode-Assembly (MEA) system was utilized throughout all experiments.

Briefly speaking, the MEA catalyst layer is a porous composite of Pt/C catalyst and a polymer electrolyte. The catalyst layer fabrication process typically involves preparation of a catalyst ink or paste depending on the subsequent application. A paste of graphite, platinum and Nafion solution is coated on one side of a piece of Nafion membrane. It is then hot-pressed to achieve a desired platinum loading by evenly distributing the paste on the Nafion polymer substrate. This assembly is commonly used in PEM fuel cells and has been used as both electrode and catalyst in other biofuel cell applications. In our experiments, to obtain an acceptable comparison between biofuel cells with different membranes, all parameters including the catalyst loading are to be fixed. Hot-pressing the paste leads to catalyst lost as well as uneven catalyst distribution. According to the analysis, adhesion of such paste depends on hydrophobicity or surface morphology of the membrane. Additionally, some polymer membranes may not be able to withstand the optimized hot-pressing temperature, which is over 100 degrees Celsius. By considering all of the constraints above, we adopt the carbon cloth coated with a fixed amount of platinum loading. It has been experimentally proven that adhesion of carbon black, platinum and carbon cloth substrate is reliable as long as no residual black powder can be viewed by naked eyes after the experiment. By using such an assembly, a fixed amount of catalyst is feasible and the carbon cloth substrate serves as a gas diffusion layer in cathode as well.

4.1.3.1. Introduction to AEM

Three different anion exchange membranes were selected (4 samples were tested as one membrane was available in two different thickness). Fumasep AEM is based on crosslinked polypropylene substrate the membrane thicknesses were 0.0355mm and 0.0812mm, for the unreinforced and reinforced membrane, respectively. AMI-7001 was 0.4622 mm in thickness and was fabricated from gel polystyrene crosslinked with divinylbenzene. The last membrane tested was Excellion Snowpure AEM, with a thickness of 0.353 mm and was made of polypropylene binder from a solventless method. The structures of AEM are different but pertinently all serve the same purpose: to allow the selective transport of anions. The open circuit voltages were recorded after the injection of electrolyte into the anode chamber and time zero in the pH measurement corresponds to the moment when GOx was added. The IV test was carried out on all membranes. Experimental results showed that a five minute wait was sufficient to obtain a stabilized current and voltage value.

4.1.3.2. AEM pH Result

The pH/time relationship of an AEM fuel cell is graphed in figure 4.4.

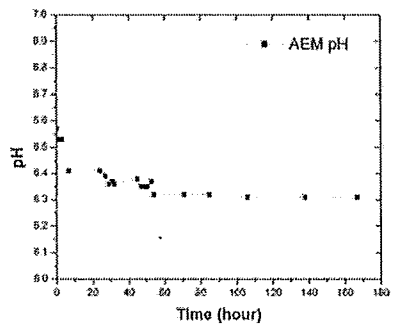

Figure 4.4 pH in an AEM based enzymatic fuel cell and time

By comparing figure 4.4 with figure 4.1, pH level of the anolyte in AEM based glucose/oxygen system dropped fast only during the first day of the experiment. The pH then dropped relatively slowly over the following 140 hours. It may be concluded that the pH has reached its steady state of proton concentration towards the

end of the experiment. As proposed in chapter 2, glucose activity is hindered by low pH environments and therefore fewer protons are produced. Consequently, slower oxidation reaction leaves sufficient time for the reaction of OH- penetration from cathode to anode as well as the neutralization of hydroxyl and proton in equation (2.24). This is to be expected, as these two effects cancel each other to reach an equilibrium state (or an equilibrium proton concentration). Thus a steady state of power output is realized. Figure 4.1 shows a constant pH drop right after time zero and gives no indication of stabilizing even towards the end of the experimental period (180 hours after time zero). On the other hand, figure 4.4 shows that an almost constant pH is successfully maintained.

4.1.3.3. I-V Performance and Internal Resistance of AEM

As explained in detail in chapter 2, a pH gradient is believed to be the hindrance of higher power density in a Nafion based biofuel cell. Our proposed AEM alternative produces consistent results for the pH level. Further tests evaluating electric performance have to be conducted. Figure 4.5 shows AEM based biofuel cells and the Nafiion based biofuel cells' open circuit voltage with respect to time. Figure 4.6 shows the IV curves of all the biofuel cells tested and figure 4.7 is the power density and current density measurement based on a 6.2 cm^2 active electrode area.

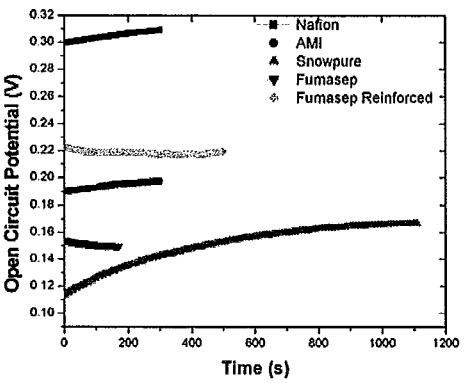

Figure 4.5 Open circuit voltage and time

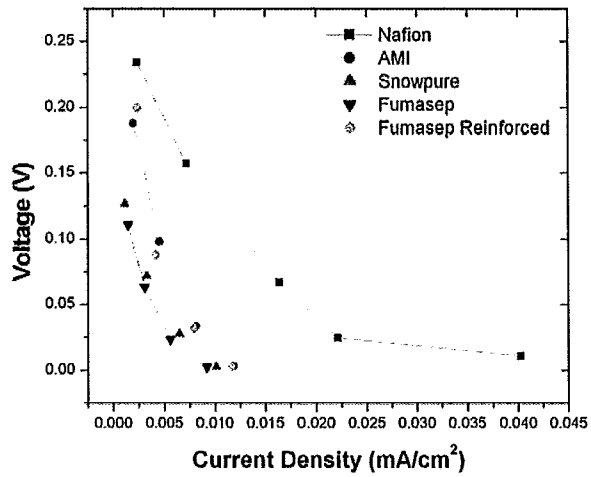

Figure 4.6 Voltage and current density

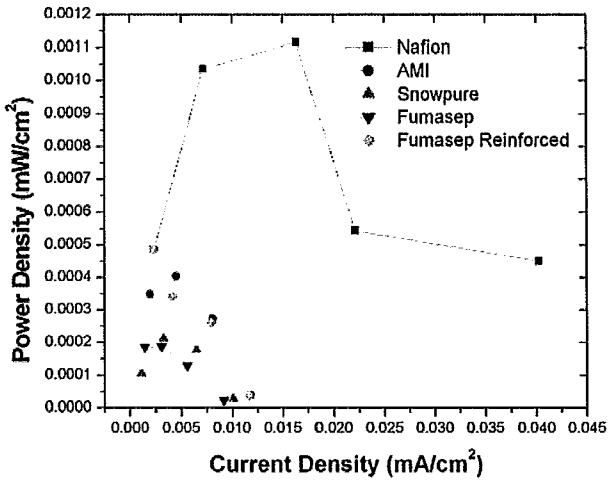

Figure 4.7 Power density and current density

It is obvious that in all 3 figures above, the black dotted line, which represents Nafion, shows the highest open circuit voltage, current density and power density. It is shown that the Snowpure based biofuel cell takes the longest time to stabilize in terms of open circuit voltage and it also shows the lowest power density.

This observation contradicts the proposed mechanism for AEM based biofuel cells. It can be seen that AEM based biofuel cells are not as good as the Nafion based biofuel cell, despite the fact, that the Nafion is hindered by the development of a pH

gradient. Further analysis was done on the I-V curve (also known as a polarization curve). The slope of a polarization curve is the total resistance (also called apparent resistance) of a biofuel cell for the corresponding current density range. This total resistance includes all internal loss caused by activation, ohmic and concentration overpotentials. The I-V curve is not a straight line and the apparent internal resistance is therefore a function of current density according to figure 2.2. In the linear region on the polarization graph, it has been suggested by Liang et al. [61] that ohmic represents a fixed ratio of the overall resistance. At the same time, ohmic resistance consists of two parts. The first part is caused by protons/hydroxyls motion in the electrolyte and the membrane. The other one is caused by the mediator/enzyme electron transportation in the electrolyte and the transportation of electrons in the external circuit. Electron transportation at the anode is accomplished by the shuttling mediators between the anode and the bulk of the electrolyte. Since identical electrolyte and mediators were used throughout all biofuel cell experiments, resistance of different membranes becomes the only element that has not been controlled.

	Nafion	AMI	Fumasep	Fumasep (Reinforced)	Snowpure
Overall Resistance(Ω)	1669	2663	3314	4458	2879

Table 4.1 Overall resistances for different membranes

Table 4.1 lists the apparent resistance for each biofuel cell based on different membranes. In the ohmic-resistance dominated region of the polarization curve, the Nafion based biofuel cell shows the lowest overall resistance and all other AEM based biofuel cells have significantly higher overall resistance. This is part of the reason why all AEM based biofuel cells give poorer power output: a higher internal resistance caused by membrane constitutes most of the ohmic loss.

Nafion and all of the AEM have no specific selectivity on the types of ions that are diffusing through them. For instance, ion conductivity for Na^+ and K^+ in

Nafion are of the same value and ion conductivity for SO_4^{2-} and PO_4^{3-} in all AEM are virtually the same. An impedance test result based on 1 cm^2 of each membrane is measured in 1 mol/L Na_2SO_4 electrolyte. It is therefore reliable to compare the ion conductivity for each different membrane using Na_2SO_4 as an electrolyte. The Nyquist plot drawn in figure 4.8 is solely from resistance behaviours of membranes themselves. The high frequency region on the Nyquist plot is indicative of only the ohmic resistance of the test samples.

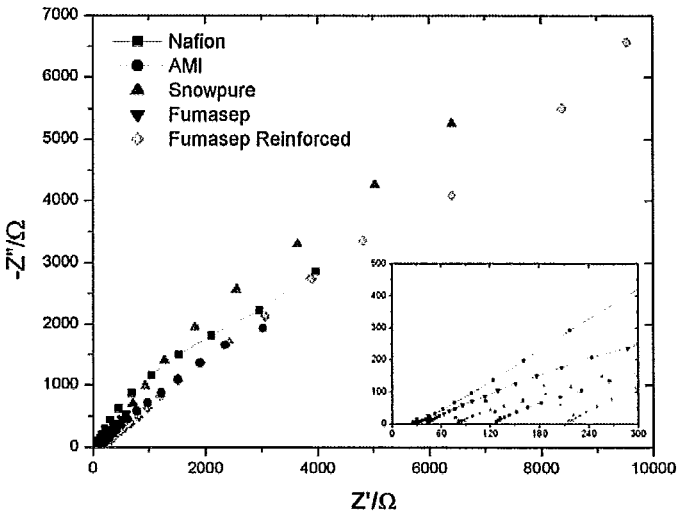

Figure 4.8 Nyquist plot for all membranes

The behaviour on the lower right corner of Figure 4.8 shows that Nafion (represented by squares), possesses the shortest distance between origin and its intersection with Z' axis. Meanwhile, the intersection of reinforced Fumasep AEM (represented by the diamond shape), shows the largest Z' intercept. The high resistance of reinforced Fumasep is consistent with the result from the polarization curve in figure 4.6. All results in figure 4.8 are significantly lower than the results in table 4.1. This is because the measurements in figure 4.8 do not include any ohmic resistance caused by junctions between different phases in our biofuel cells or the loss caused by activation overpotential. Moreover, the effective area of the test sample as well as the electrolyte in impedance test should be taken into consideration. It is well

accepted by many researchers [62] [34] that the membrane in a PEM fuel cell comprises a large portion of the total ohmic resistance. Therefore it is not surprising that membranes, especially those with higher resistances, such as the AEM, also provide the most ohmic resistance in a biofuel cell. Nafion as the membrane in a biofuel cell is inherited from commercialized PEM fuel cells. It is therefore self-evident that Nafion has been selected partly due to its low resistance.

As a summary of the polarization curve and Nyquist plot above, AEM successfully suppressed proton accumulation in anode, which is thought to be the bottleneck in biofuel cells. However, AEM biofuel cells could not yet resolve problem of low power density, this is due to the fact that they introduces another issue: higher membrane resistance. It is assumed in the first place that activation resistance as well as the capacitor-like double layer is not affected by changing the membranes to AEM in a biofuel cell. An internal circuit for a microbial fuel cell was proposed by adopting internal circuit from earlier PEM fuel cells as shown in figure 4.9 by Liang et al. [61]. This is exactly the same as the circuit shown in figure 2.12 and is currently the only proposed internal circuit for biofuel cells to the best of the authors' knowledge. Subscripts a and c in figure 4.9 represents elements in the anode and the cathode. The experiments in the following section are done with the intention of validating this model.

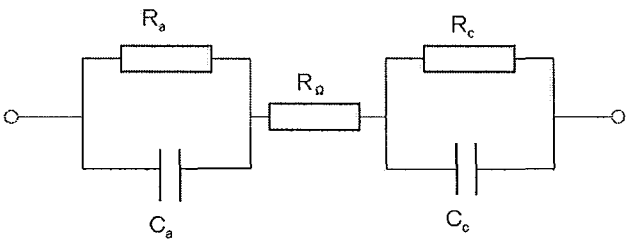

Figure 4.9 Proposed internal circuit for biofuel cells [61]

4.2. Further Transient Test on All Membranes

4.2.1. Load Step Measurement and RC Circuit Mode

For further analysis of the internal resistance, according to figure 2.12, a testing circuit of figure 2.14 is applied using CMS corrosion system. R_1 and R_2 were 10KΩ and 50Ω respectively in figure 2.12 and they were used as an external resistance before and after load switch. At time t=0, the external load is connected from open circuit to the parallel combination of R_1 and R_2. At time t=1000 seconds, the overall external resistance switches to R_1 alone. 1000 seconds provided an adequate period of time for the stabilisation of the current curve. 10KΩ and 50Ω were chosen only because they corresponded to two points in the linear portion of the polarization curve shown in figure 4.6. A large difference in value was chosen as to optimize the separation of each point along this curve. The reason for the resistances must be on the linear region of the polarization curve will be discussed in section 4.2.2.

According to the model by Liang et al. [61] in figure 4.9, at the time of load switch (at both t=0 and t=1000), the capacitor in the circuit which arises from electrochemical double layer, charges or discharges. The total time of charge and discharge is a function of the capacitance and the resistance. In order to characterize the corresponding capacitance in the equivalent circuit, the calculation for the model has to be reviewed. This is achieved prior to the analysis by introducing a similar simplified electric circuit as follows:

A simplified RC model for the DC circuit in figure 4.9 is drawn in figure 4.10.

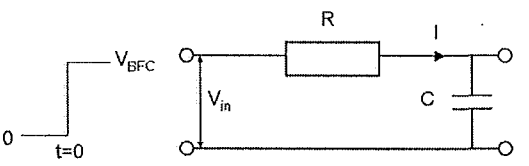

Figure 4.10 Basic RC circuit model during charge

At time t=0, V_{in} is equivalent to zero. There is no current in the circuit and no voltage drop across any the resistor (V_R) or capacitor (V_C). Immediately proceeding time t=0, V_{in} suddenly increases to V_{BFC}, the open circuit voltage of our biofuel cell and the current going through the circuit (I) starts to change. By applying Kirshoff's current law, the current going out of the resistor (R) is the same as the current going into the capacitor (C):

$$C(dV_C/dt)=I=V_R/R \quad (4.1)$$

$$V_{in}=V_C+V_R \quad (4.2)$$

Therefore: $$V_{in}-V_C= RC(dV_C/dt) \quad (4.3)$$

By solving this differential equation, using the boundary conditions such described above (i.e. B.C. V_C=0 when t=0) the current I and voltage across the capacitor are:

$$V_C=V_{in}[1-exp(-t/RC)] \quad (4.4)$$

$$I=I_0exp(-t/RC) \quad (4.5)$$

Where $$I_0= V_{BFC}/R \quad (4.6)$$

And $$\tau=RC \quad (4.7)$$

Solution (4.5) for current is given during charge of the capacitor because by applying the boundary condition, it is obvious that current reaches its maximum at t=0. The initiation of the current flow following t=0 corresponds to the building up of charge on the double layer (the capacitor in our model). Time constant τ, determined by the product of R and C, is used to represent a time scale for the charge and discharge behaviour in the circuit above.

$$I=I_0(1-exp(-t/RC)) \quad (4.8)$$

Similarly, once the voltage source is removed from the circuit, the charge stored on the capacitor begins to move backwards through the circuit. Schematically, the current behaviour, expressed in equation (4.8), is a symmetrical image of equation (4.5). Current in equation (4.8) increase dramatically in the beginning and the rate of change of the current drops significantly as time goes by. It is a mathematical

estimation that the capacitor is fully charged or discharged after approximately t=5τ.

4.2.2. Load Step Measurement

The model in the section above explains the current behaviour during the charge and discharge of the capacitor in the equivalent circuit. According to the experimental details in 4.2.1, current behaviours after load switch are measured. Figure 4.11 is a comparison of the five biofuel cells based on different membranes discussed in 4.1. These experiments were conducted at 18 degrees Celsius using the load step method. In the following analysis, t1 and t2 correspond to the time after the initial charge (t=0) and after the discharge process (t=1000) respectively.

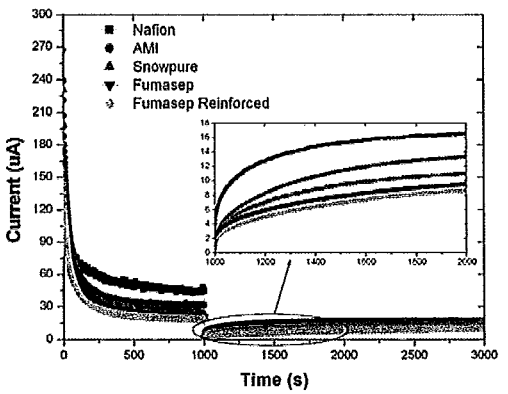

Figure 4.11 Load step measurement for all membranes at 18 degrees Celsius

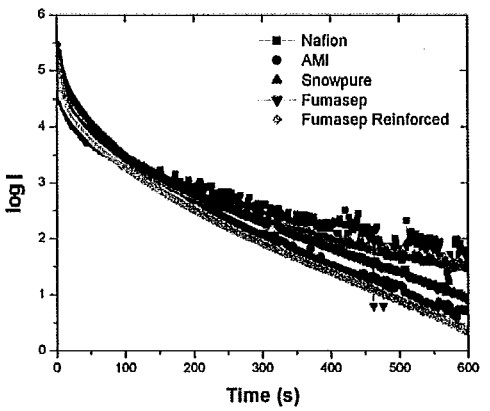

Figure 4.12 Time constant 1 for all membranes at 18 degrees Celsius

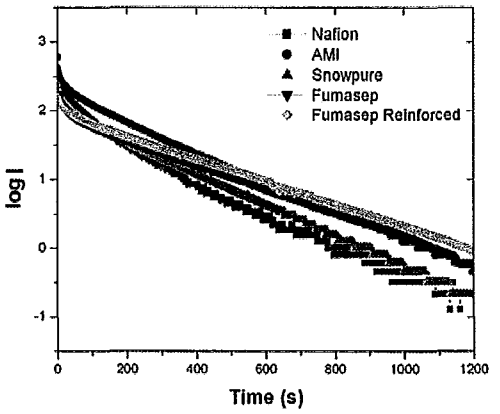

Figure 4.13 Time constant 2 for all membranes at 18 degrees Celsius

In figure 4.11, the current apparently exhibits a fast ohmic drop followed by a slower relaxation towards the new steady state. An enlarged figure on the lower right corner describes the curves after the load switch. Less importantly, the black line representing Nafion is still on top of all other curves. The Nafion still exhibits the highest power density among all biofuel cells before and after the load switch. Before t=1000 seconds, an equilibrium with relatively high current density was established. At t=1000 second, the fuel cells starts to build another equilibrium at a smaller current density. The transition can be illustrated below in figure 4.14 on the polarization curve.

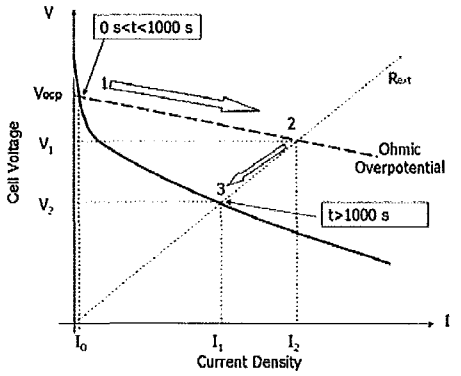

Figure 4.14 Polarization curve and load step test

The two equilibriums mentioned above are point 1 and 3 in figure 4.14. Upon switching at t=1000 seconds, the circuit instantaneously moves from point 1 to point 2. Afterwards, it slowly shifts to point 3 because of the presence of electric double layer(s). The slope of the straight line R_{ext} is the sum of overall external resistance and the dashed line between 1 and 2 corresponds to ohmic overpotential loss.

Mathematically, by choosing the base lines for t1 and t2, we are able separate the 2 exponential terms using equation (4.3) and (4.6). Taking the logarithm of relative currents results in the relationship between the relative current and the time constants (RC) in equation (4.7) and (4.8). This is graphically represented in figure 4.12 and 4.13. The subscript 1 and 2 after τ correspond to the discharge and charge process respectively.

$$log\ (I/I_0) = -t/RC \tag{4.7}$$

$$log\ (1- I/I_0) = -t/RC \tag{4.8}$$

	Nafion	AMI	Fumasep	Fumasep(reinforced)	Snowpure
τ_1(sec)	336	220	225	190	289
τ_2(sec)	446	488	564	617	448
C(mF)	11.06	26.93	34.07	42.91	15.97

Table 4.2 Time constant and capacitance for all membranes at 18 degrees Celsius

The overall internal resistance is estimated by measuring the slope of the polarization curve in figure 4.6. It is clear that 50Ω and 10KΩ are included in our polarization curves and the curves are highly linear in this region. In fact, a small deviation on the slope can make a huge difference on the value of internal resistance. Therefore it is not accurate enough to calculate overall capacitance using this estimate of the slope. However, it is still valid to assume that the overall internal resistance is a constant between the externally applied resistances from 50Ω to 10KΩ, due to the shape of the polarization curve. Moreover, the double layer capacitance is determined by thermodynamics and it is not a function of current density. Therefore we may assume a fixed capacitance value before and after load switch. Thus for a same

biofuel cell at a fixed temperature, one can apply the two conditions to solve for the equation (4.5):

$$(50+R_i)C=\tau_1 \quad (4.9)$$

$$(10000+R_i)C=\tau_2 \quad (4.10)$$

By solving the equations above, the results of C, the overall capacitance from double layer is listed in the last row of table 4.2.

It is obvious that AMI and Fumasep based biofuel cells show relatively higher overall capacitance than Nafion based biofuel cells. Snowpure based biofuel cells exhibit slightly higher overall capacitance than Nafion based biofuel cells. The earlier assumption of changing membranes without affecting electrical double layer has to be corrected. The overall resistance is slightly affected by the membranes that are placed between anode and cathode in a glucose/oxygen enzymatic biofuel cell. It is inconclusive that the membrane would alter the structure of electrochemical double layer and the mechanism for such behaviour is unknown. All AEM based biofuel cells build up a larger electrochemical double layer. In this particular case, the simple internal circuit model in figure 4.9 which is directly inherited from PEM fuel cells would appear to be inadequate to describe the mechanisms of a biofuel cell.

In the PEM fuel cells, the above model dominates almost all PEM fuel cell research, and this arises from its simple yet important structure. Hydrogen is pumped in and separated by a platinum catalyst at the electrode-gas-catalyst triple phase interface. This is one of the two places in a PEM fuel cell that can generate an electrical double layer. Therefore, no more than 2 capacitors are found in a PEM fuel cell exactly as modeled in figure 4.9. However, a biofuel cell involves multiple steps of redox reactions and hence increases the complexity of the system significantly. A biofuel cell in general, can be viewed as a PEM fuel cell system by adding sophisticated biological redox reactions at the anode.

To further study the double layer and internal structure, transient load step

measurements were carried out for two fuel cells based on PEM and AEM technology at different temperatures. The results of these experiments are shown in the following section.

4.3. Temperature Dependence on Time Constant

Load step experiments were conducted at 18 and 30 degrees Celsius using the same external resistances as described in the last section. The temperature of 30 degrees Celsius was selected because GOx activity shows a maximum value at 30 degree Celsius according to Sahmetlioglu et al. [67] in figure 4.15.

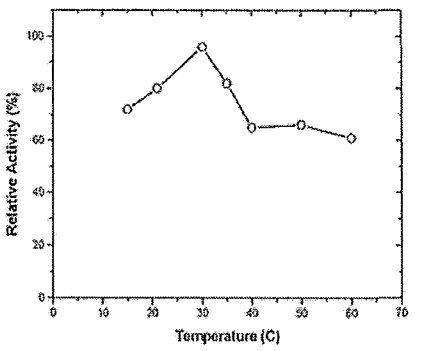

Figure 4.15 GOx activity and temperature [67]

Figure 4.16 and 4.19 show the original charge accumulation and relaxation before and after t=1000 seconds at 18 and 30 degrees Celsius respectively. Figure 4.17, 4.18, 4.20 and 4.21 graphically represent the logarithm of the relative current density versus time. The same calculation method as described in the section above was used to determine time constants and their corresponding overall resistance. The results of these calculations are shown in table 4.3.

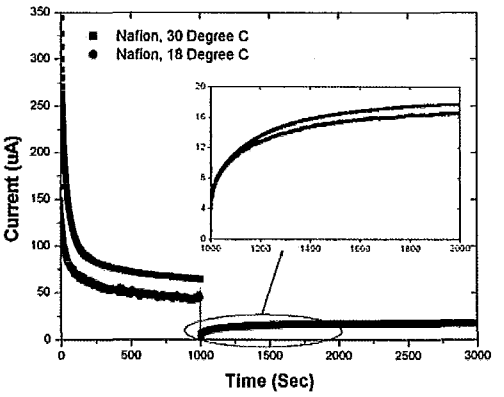

Figure 4.16 Step load measurement for Nafion at 18 and 30 degrees Celsius

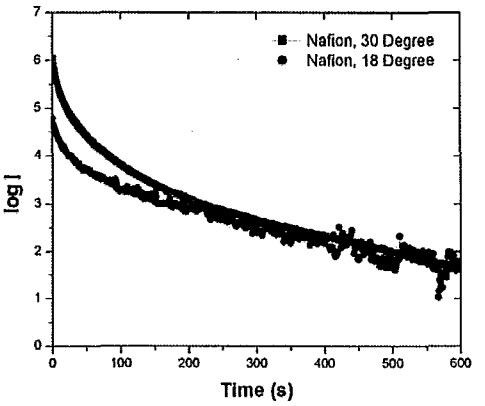

Figure 4.17 Time constants 1 for Nafion at 18 and 30 degrees Celsius

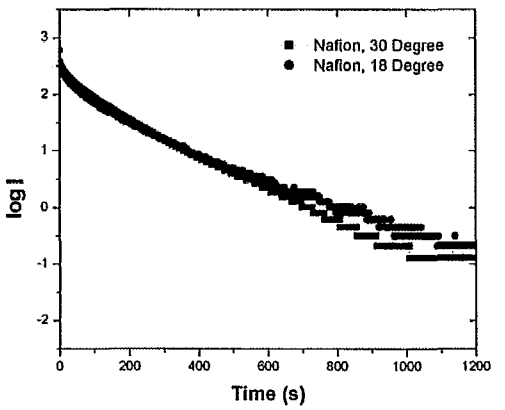

Figure 4.18 Time constants 2 for Nafion at 18 and 30 degrees Celsius

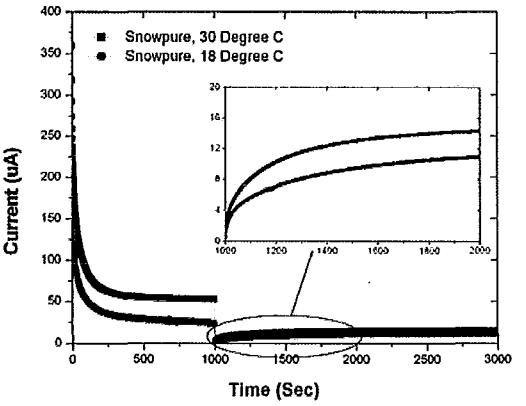

Figure 4.19 Step load measurement for Snowpure at 18 and 30 degrees Celsius

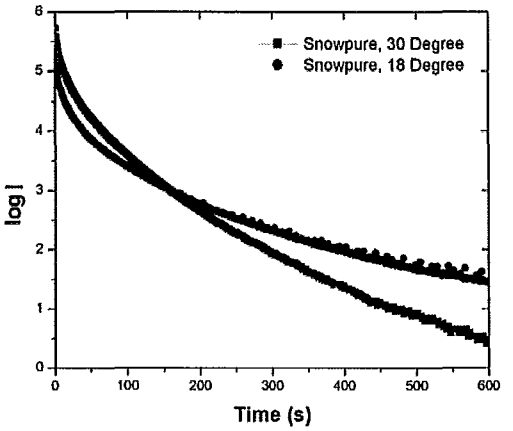

Figure 4.20 Time constants 1 for Snowpure at 18 and 30 degrees Celsius

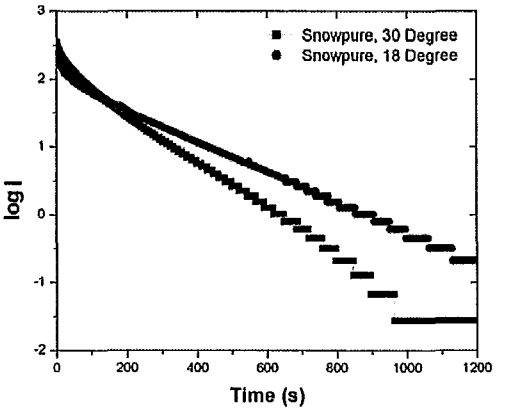

Figure 4.21 Time constants 2 for Snowpure at 18 and 30 degrees Celsius

	Nafion			Snowpure		
	τ_1(sec)	τ_2(sec)	C(mF)	τ_1(sec)	τ_2(sec)	C(mF)
18 Celsius	336	446	11.06	289	448	15.98
30 Celsius	287	355	6.83	233	296	6.33

Table 4.3 Time constants and capacitance for Nafion and Snowpure at 18 and 30 degrees Celsius

As observed in figure 4.16 and 4.19, it is not surprising that by increasing temperature from 18 to 30 degrees Celsius, a higher power density is obtained. The effect of the change in temperature on the Nernst equation, expressed in equation (2.5) has a negligible effect on the power output. It is consistent to believe that the relationship in figure 4.15 plays an important role on the increase of power output. However, our primary concern with regards to the power output, rather the relationship between the time constants and temperature. For both membrane based biofuel cells, drops in total capacitance are observed by warming the fuel cell to 30 degrees Celsius as shown in table 4.3. Again, according to the model in figure 4.9, the enzymes with higher activity will not affect the structure of the electrochemical double layer. There must be a hidden reason which has an impact on the internal circuit of our glucose/oxygen biofuel cells. A decreased capacitance value is evidence that the internal double layer may be affected by enzymes which are evenly distributed in the electrolyte.

4.4. Further discussion on biofuel cell model

4.4.1. Model for PEM

4.4.1.1. Transient State and PEM Model

Scientifically, the core of a PEM fuel cell structure is a membrane being sandwiched by two electrodes and catalysts. Most books [64] [33] or review papers [63] only give an overview of the energy conversion diagram at the steady state. Hydrogen gas is separated at the anode into electrons and protons and they recombine

to form water at the cathode. Ions and electrons are moving in different paths to generate electricity in external circuit and double layers cause irreversible voltage loss. It looks as if this gives a complete explanation of the PEM fuel cells mechanisms. However, the origin and function of the double layer can not be fully understood without considering how the reaction is initiated. The books and papers mentioned above offer details regarding engineering aspects of all elements in PEM fuel cells. For instance, catalyst morphology, water management, system build-up, structures of electrode slabs are intensively explained up to the most recent technology. One could still remain confused, from a physics point of view, as to how the first proton manages to go through membrane to the cathode. One could still remain confused, form energy point of view, where the activation overpotential is consumed. A detailed structure of catalyst assembly as well as energy diagram is drawn in figure 4.22.

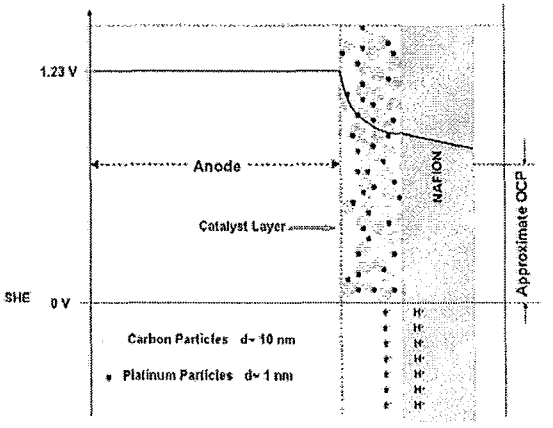

Figure 4.22 Internal energy drop in a PEM fuel cell

The graph illustrates the energy loss with respect to standard hydrogen electrode (SHE) at the anode. The grey dots adjacent to Nafion membrane constitute the gas diffusion layer or catalyst layer. They are carbon particles in about 10 nm in diameter. The black platinum particles are several nanometers in diameter and are attached to the carbon particles. With respect to SHE, the output voltage from a thermodynamic calculation is 1.23 volt. An exponential drop in the potential of the

electron is caused by the activation overpotential is observed in the triple phase region. A linear drop in potential is observed in the Nafion layer, and it is caused by ohmic losses. The overall open circuit potential (OCP) drops further at the cathode. This will not be discussed as it is adequate to understand the initialization in PEM fuel cells by considering behaviour only at the anode. This is a result of the fact that cathode activation loss is in symmetry with anode activation loss. A detailed diagram of the cell before connecting an external circuit is drawn below in figure 4.23.

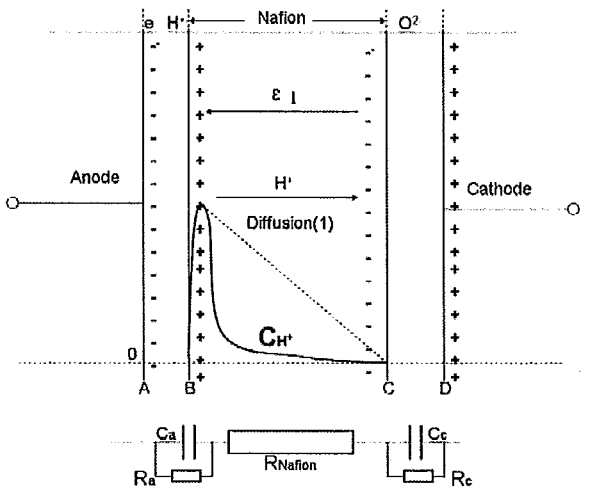

Figure 4.23 Transient charge distributions in a PEM fuel cell without external circuit

In figure 4.23, upon the injection of hydrogen, an equilibrium between hydrogen and protons and electrons is established. Only protons can move freely towards Nafion because of Nafion's selective ionic conductivity. A distribution of proton concentration is therefore built and it is represented by the red solid curve in figure 4.23. A similar process takes place at the cathode and it only changes from hydrogen to oxygen. The red plus and minus signs, representing a double layer on the Nafion, are the cause of the black double layer (+ and -) on the outer sides of the electrodes. Electrons on the catalyst layer are not able to travel through Nafion, because of Nafion's selectivity. Electrons are not able to travel to the external circuit as well, due to an open circuit condition. Accumulation of electrons at the electrode as

well as the accumulation of protons on the surface of Nafion builds the double layer. The apparent voltage ε_1 is measured from point A to point B and it is numerically the OCP for the PEM fuel cell in figure 4.23. Proton diffusion in figure 4.23 is fast because of the large proton gradient across the membrane. This gradient becomes linear before a stable OCP is established. The proton distribution at equilibrium is graphically represented by the red dash line in figure 4.23.

4.4.1.2. Steady State and PEM Model

After the connection of external circuit, figure 4.23 becomes figure 4.24.

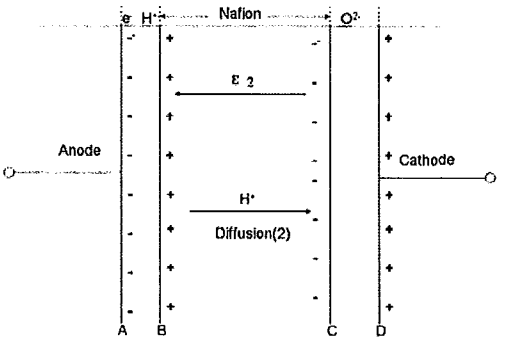

Figure 4.24 Internal charge distributions in a PEM fuel cell with external circuit

In a working PEM fuel cell with an external load, charge density on all interfaces, as illustrated in figure 4.24, is smaller than charge density in figure 4.23. The direction of electric field ε_2 is the same as ε_1 in figure 4.23 but smaller in magnitude. The net difference between ε_2 and ε_1 is the sum of all overpotentials. Activation overpotential is not wasted, as it lowers the energy barrier for the conversion from hydrogen to protons and electrons.

4.4.2. Model Discussion in Biofuel Cells

A simple estimation of active surface area of the electrical double layer can be conducted as follows. The calculation is based on a PEM fuel cell with a total platinum loading of 0.1 gram. Xu et al. [68] in 2007 calculated the active surface area

of platinum in PEM fuel cells and approximated that 20%-70% of the platinum was active. A typical catalytic platinum particle size of 2 nm reveals a total active area of 127 m^2/g [69]. With an average of 20% and 70% active platinum, a total surface area of 32 m^2 can be approximated for the PEM fuel cell described above. The equation for calculating capacitance is as follows in equation (4.10). Where ε is the dielectric constant, A is the active area and d is distance between the double layers.

$$C=\varepsilon A/d \tag{4.10}$$

We assume d is of the magnitude of an Angstrom because of the surface geometry illustrated in figure 4.22. The dielectric constant is 8.85e-12 F/m for vacuum at 20 degrees Celsius. By taking the surface morphology into account, hardly anything can exits between the platinum particles and the carbon particles. Therefore, using the dielectric constant for vacuum or air (very similar to vacuum) is acceptable. Subsequently, the capacitance calculated from equation (4.10) is 3 to 5 F. This value is in agreement with Larminie et al.'s [33] result.

A similar approximation to the one described above was conducted for a biofuel cell. According to table 4.2 and 4.3, the capacitance for a biofuel cell is in the range from 10 mF to 50 mF. We can hereby estimate the totally active area using the same assumptions as for the PEM fuel cell. One condition that has changed between the two systems is the dielectric material between the double layers. Phosphate buffer solution is used to provide a physiological condition for the biological reaction. The true relative dielectric constant of the dielectric material in the biofuel cell is slightly higher than that of vacuum but smaller than that of water (which is 80). However, since we have confined the distance to the angstrom scale, this distance can hardly store any buffer solution molecules and the dielectric constant for air or vacuum may be used. Alternatively, if the distance is increased to the nanometer scale and consequently a higher value is assigned for the dielectric constant, the capacitance remains almost the same. Ironically, the ratio of d/ε is in the same order of magnitude in both approximations. As a result, the selection of the dielectric constant and the

distance between the double layers would not affect the final result. By substituting the appropriate values into equation (4.10), we surprisingly end up with an active area of 500 to 2500 cm^2. This value is more than 100 times larger than the surface area of the electrode in our biofuel cell: 6.2 cm^2. It is conclusive evidence that an unrevealed active area has contributed to electrochemical processes in the biofuel cell reaction.

A detailed energy diagram as well as oxidation process is drawn in figure 4.25

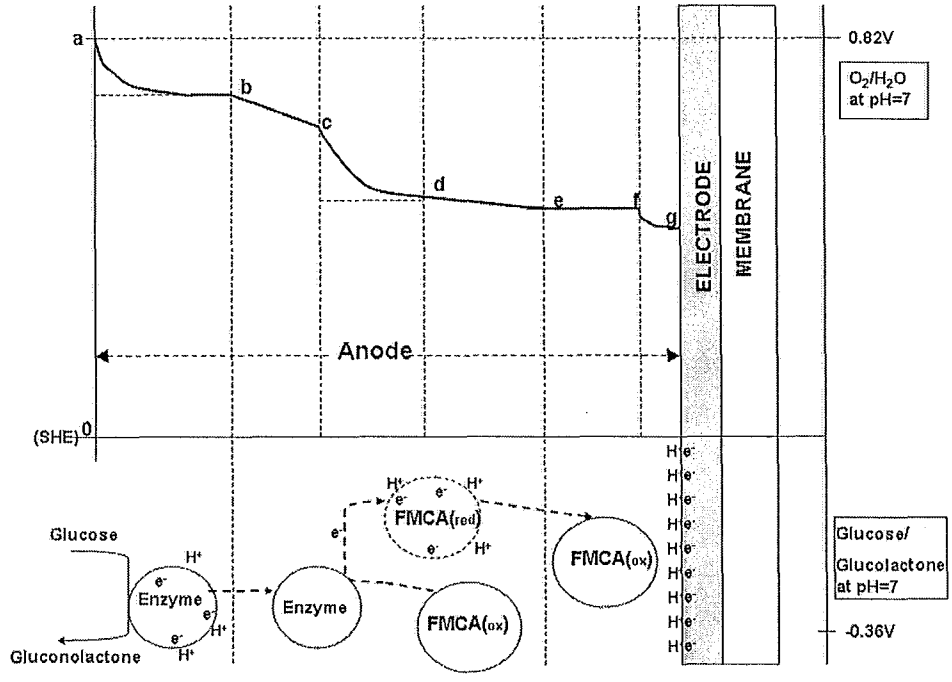

Figure 4.25 Energy drop in a Glucose/oxygen enzymatic biofuel cell

With respect to SHE, the reaction of oxidation from glucose to gluconolactone provides an OCP of 1.18V (0.82V+0.36V). In the anode chamber, three exponential energy drops, namely ab, cd and fg in figure 4.25 are observed. They are the proposed activation losses caused by the double layers and they are in exponential form. The enzymes which absorb electrons and positively charged ions are distributed in the electrolyte. These ions are not necessarily the protons as seen in figure 4.25; the concentration of these cations is higher near the surface of the enzyme. The result of cation build up is the proposed liquid phase double layers. These liquid phase double

layers can be observed everywhere in the electrolyte. However, they are not necessarily distributed uniformly in the electrolyte. A higher concentration of liquid phase double layer can be found near the electrode because of the dissipation of protons through the membrane. A similar double layer has been proposed for FMCA, the mediator. Mediator molecules take the electrons from the enzyme molecules and shuttle to the electrode. As long as there are absorbed electrons on the surface of FMCA molecules, the electrons and the cations in the electrolyte react to form a double layer. The curve illustrated by the drop at fg in figure 4.25 is the original double layer formed at the electrolyte and electrode interface. Straight lines bc and de represent the ohmic losses during electron transportation in the electrolyte.

An internal equivalent circuit for an enzymatic biofuel cell should meet all the requirements below. First of all, by using multiple electric circuit elements, the model should adequately describe the transient behaviour illustrated above. Secondly, it should adequately describe the transition between the transient state to the steady state. The model in figure 4.9 and 4.23 are not capable of explaining system transition from transient to steady state. Thirdly, more than one process in a biofuel cell can result in double layers and therefore a multiple-capacitor structure is a must. Last and possibly the hardest, it appears from the model described by figure 4.25 that all double layers are in series because of the sequence of reactions. In fact, capacitors in series will reduce the total capacitance and therefore end up with smaller relaxation effect in the transition. It is clear that the total capacitance is much larger in our biofuel cells than it is in PEM fuel cells. As a result, the equivalent circuit has to be in series in steady state and in parallel during transient period.

5. Conclusions

In this thesis, solutions to the problem of low power density caused by pH deviation in the anode and the cathode of a glucose/oxygen based enzymatic fuel cell using GOx and FMCA were provided. The alternative solutions proposed have caused other complications to the system by reducing the pH gradient. Moreover, a conclusive result of a large active area in an enzymatic biofuel cell was determined by a transient state study and the complete process of electrical double layer formation was described.

The low power density of the biofuel cells was caused by the hindrance of proton transportation due to cations from the alkaline based buffer solution. A side effect of this behaviour was the establishment of a pH gradient in the anode and cathode chambers. A survey of possible solutions to the above problem was conducted and two feasible alternatives were suggested. The first alternative, using Tris buffer with no alkaline ion was rejected due to the fact that it caused a larger pH gradient than observed when using a phosphate based buffer solution. The second alternative: using anion exchange membrane (AEM), successfully resolved issues pertaining to the pH gradient. The pH gradient is widely considered a bottleneck in biofuel cell development. Unfortunately, all of the AEM biofuel cells showed relatively lower power density than the Nafion based enzymatic biofuel cells. It was proven that this is the result of relatively high internal resistance in the AEM membranes as compared to the Nafion membrane.

A Transient study was initiated to conduct further experimentation and analysis of the internal resistance of AEM based biofuel cells. A discrepancy was found when applying the rarely-mentioned internal circuit model to biofuel cells. Firstly, by examining the capacitance data of a PEM fuel cell using a well-established

internal circuit produced results which are consistent with literature. The capacitance caused by the electrochemical double layers is in the same order of magnitude as has been adopted by other researchers. However a much larger surface area than our electrode was found by applying the identical estimation to our biofuel cells. It was therefore concluded that the proposed electrical chemical double layers were in the electrolyte as well as at the interface of the electrodes. Otherwise, the two-dimensional electrode would have to comprise a surface area several hundreds times larger than the electrode itself. Last but not least, based on the assumption that double layer can be found on enzymes and mediators in the electrolyte, a detailed description of electron/proton double layers found on the enzymes and mediators in the electrolyte were given.

A complete list of requirements for the equivalent circuit was portrayed for our glucose/oxygen enzymatic biofuel cells using GOx and FMCA. This equivalent circuit points to a possible direction for future biofuel cell research.

This work represents a step towards a more comprehensive understanding on enzymatic biofuel cells. Guided by a better fundamental understanding of the formation and dissipation of double layers and their corresponding activation losses, improvements to the power output can be made to enzymatic biofuel cells.

Reference

[1] Shukla, A. K.; Suresh, P.; Berchmans, S.; Rajendran, A. *Current Science* **2004**, *87*, 25.

[2] Bullen, R.A.; Arnot, T.C.; Lakeman, J.B.; Walsh, F.C. *Biosensors and Bioelectronics* **2006**, 21, 2015

[3] Dixon, B.; *Biotechnology* **1984**, *2*, 921.

[4] Yao, S.J., Appleby, A.J., Geise, A., Cash, H. R., Wolfson, S.K. *Nature* **1969**, *4*, 73.

[5] Bennetto, H.P.; Dew, M.E.; Stirling, J.L.; Tanaka, K. *E. coli. Chem. Ind.* **1981**, *7*, 776.

[6] Thurston, C.F.; Bennetto, H.P.; Delaney, G.M.; Mason, J.R.; Roller, S.D. *J. Gen. Micribiol.* **1985**, *131*, 1393.

[7] Logan, B. E.; Hamelers, B.; Rozendal, R. *Environ. Sci. Technol.* **2006**, *40*, 5181.

[8] Cheng, S.; Liu, H.; Logan, B.E. *Electrochem. Commun.* **2006**, *8*, 489.

[9] Rabaey, K.; Lissens, G.; Siciliano, S. D.; Verstraete, W. *Biotechnol. Lett.* **2003**, *25*, 1531.

[10] Topcagic, S.; Minteer, S. D. *Electrochimica Acta*, **2006**, *51*, 2168.

[11] http://www.sony.net/SonyInfo/News/Press/200708/07-074E/index.html

[12] Roller, S.S. *J. Chem. Technol. Biotechnol.* **2006**, *34*, 3.

[13] Nevin, K.P.; Lovely, D.R. *Appl. Environ. Microbiol.* **2002**, *68*, 2294.

[14] Barton, S.;Gallaway, S.; Atanassov, P. *Chem. Rev.* **2004**, *104*, 4867.

[15] Chaudhuri, S.K,; Lovely, D.R. *Nature Biotechnol.* **2003**, *21*, 1229.

[16] Kim, H.J.; Park, H.S.; Hyun, M.S. *Enzyme Microb. Technol.* **2002**, *30*, 145.

[17] Park, H.S; Kim, B.H,; Kim, H.S. *J. Anaerobe.* **2001**, *7*, 297.

[18] Pham, C.A.; Jung, S.J.; Phung, N.T. *J.FEMS Microbiol. Lett.* **2003**, *223*, 129.

[19] Park, D.H.; Zeikus, J.G. *Appl. Environm. Microbiol.* **2000**, *66*, 1292.

[20] Kim, N.; Choi, Y.; Jung, S. *J. Biotechnol. Bioeng.* **2000**, *70*, 109.

[21] Parrondo, J.; Barrio, A.; Lombrana, J.; Mijangos, F. *Ind. Eng. Chem. Res.* **2008**, 4481.

[22] Kim, J.; Jia, H.; Wang, P. *Biotechnology Advances* **2006**, *24*, 296.

[23] Karyakin, A.A.; Morozov, S.V.; Karyakina, E.E.; Varfolomeyev, S.D.; Zorin, N.A., Cosnier, S. *Electrochemistry Communications* **2002**, *4*, 417.

[24] Pandey, P.C; Upadhyay, B.C. *molecules* **2005**, *10*, 728.

[25] Moore, C.M.; Akers, N.L.; Hill, A.D,; Johnson, Z.C.; and Minteer, S.D. *Biomacromolecules* **2004**, *5*, 1241.

[26] http://www.sony.net/SonyInfo/News/Press/200708/07-074E/index.html

[27] Haselkorn, A. Daily California, **2002** 28 Aug

[28] http://www.scientificpsychic.com/fitness/carbohydrates.html

[29] Katz, E.; Willner, I.; Kotlyar, A.B. *J. Electroanal. Chem.* **1999**, *64*, 476.

[30] Barbir, F. *Proceedings of the European Fuel Cell Forum Portable fuel cells Conference, Lucerne*, 112.

[31] Rozendal, R.A.; Hubertus, V.M.; Hamelers,; Rabaey, K.; Keller, J.; Buisman, C.J.N. *Water Science and Technology*, **2008**, *57*, 1757.

[32] Alberty, R.A. *Biochemical Education*, **2000**, *28*, 12.

[33] Larminie,J.; Dicks, A. *Fuel Cell Systems Explained*, John Wiley &Sons Ltd., West Sussex, England, **2003** 2nd ed.

[34] Wang, Y; Wang, CY. *Electrochim. Acta.* **2005**, *50*, 1307.

[35] Um, S.; Wang, C.Y.; Chen, K.S. J. *Electrochem. Soc.* **2000**, *147*, 4485.

[36] Wang, C.Y. *Chem. Rev.* **2004**, *104*, 4727.

[37] Liu, H.; Logan, B.E. *Environ. Sci. Technol.* **2004**, *38*, 4040.

[38] IUPAC Compendium of chemical Teminology, **1997**, 2nd ed.

[39] Laurencelle, F.; Chahine, R.; Hamelin, J.; Fournier, M.; Bose, T.K.; Laperriere, A. *Fuel Cells*, **2001**, *1*, 66-71.

[40] Tsujimuma. S.; Kano, K.; Ikeda, T. *Electrochemistry* **2002**, *70*, 940.

[41] Yeager, E. *Electrochim. Acta.* **1984**, *29*, 1527.

[42] St-Pierre, *J. New Mat. Electrochem. Systems* **2000**, *3*, 99-106.

[43] Strathmann, H. *Ion-exchange Membrane Separation Process*. Amsterdam, Boston, Elsevier **2004.**

[44] Abe, T.; Shima, H.; Watanabe, K.; Ito, Y. *J. Electrochem. Soc.* **2004**, *151*, A101.

[45] Gil, G.G.; Chang, I.S.; Kim, B.H., Kim, M.; Jang, J.K.; Park, H.S.; Kim, H.J. *Biosensors and Bioelectronics* **2003**, *18*, 327.

[46] Rozendal, R. A.; Hamelers, H. V. M.; Buisman, C. J. N. *Environ. Sci. Technol.*

2006, *40*, 5206.

[47] Chae, K. J.; Choi, M.; Ajayi, F. F.; Park, W. S.; Chang, I. S.; Kim, I. S. *Energy and Fuels* **2008**, *22*, 169.

[48] Katz, E; Willner, I. *Journal of the American Chemical Society* **2003**, *125*, 6803.

[49] Liu, H.; Ramnarayanan, B.; Logan, B. E. *Environ. Sci. Technol.* **2004**, *38*, 2281.

[50] Liu, H.; Cheng, S. A.; Huang, L. P.; Logan, B. E. *Journal of Power Source* **2008**, *179*, 274.

[51] Chen, T.; Barton, S. C.; Binyamin, G.; Gao, Z. Q.; Zhang, Y. C.; Kim, H. H.; Heller, Adam. *J. Am. Chem. So.* **2001**, *123*, 8630.

[52] Beynon, R.J.; *Easterby, J.S. Buffer Solutions*: *The Basics,* Oxford University Press, Oxford, New York **1996**

[53] Call, D.; Logan, B. E. *Environ. Sci. Technol.* **2008**, *42*, 3401.

[54] Rozendal, R. A.; Sleutels, T.H.J.A.; Hamelers, H.V.M.; Buisman, C.J.N. *Water Science & Technology* **2008**, *57*, 1757.

[55] Rozendal, R.A.; Hamelers, H.V.M; Molenkamp, R.J.; Buisman, C.J.N. *Water Research* **2007**, *41*, 1984.

[56] Kim, J.R.; Cheng, S.A.; Oh, S.E.; Logan, B. *Environ. Sci. Technol.* **2007**, *41*, 1004.

[57] Cheng, S.A,; Logan, B.E. *Water Science and Technology* **2008**, *58*, 853

[58] Zuo, Y.; Cheng, S.A.; Logan, B.E. *Environ. Sci. Technol.* **2008**, *42*, 6967.

[59] http://www.lanl.gov/orgs/mpa/mpa11/breakthrough1.htm

[60] Zhi, M.X. MASc Thesis, Mcmaster University **2006**

[61] Liang, P.; Huang, X.; Fan, M.Z.; Cao, X.X.; Wang, C. *Applied Microbiology and Biotechnology* **2007**, *77*, 555.

[62] Weydahl, H.; Moller-Holst, S.; Hagen, G.; Borresen, B. *Journal of Power Source* **2007**, *171*, 321.

[63] Wang, C.Y. *Chem. Rev.* **2004**, *104*, 4727.

[64] Zhang, J.J. *PEM Fuel Cell Electrocatalysts and Catalyst Layers, Fundamentals and applications*, Spinger, London, **2008**.

[65] Büchi, F.N.; Marek, A.; Scherer, G.G. *J. Electrochem. Soc.* **1995**, *142*, 1895.

[66] Newman, J. *J. Electrochem. Soc.* **1970**, *117*, 507.

[67] Sahmetlioglu, E.; Yuruk, H.; Toppare, L.; Cianga, I.; Yagci, Y. *Reactive and Functional Polymers* **2006**, *66*, 365.

[68] Johnston, C.M.; Xu, H.; Brosha, E.; Chlistunoff, J.; More, K.; Orler, E.B.;

Mawley, M.; Pivovar, B. Measurement and Understanding of Catalyst Utilization in Fuel Cells. Prime2008, *214th Meeting of the Electrochemical Society*, Hawaii, USA Oct12-17, **2008**

[69] Xu, H.; Brosha, E.; Garzon, F.; Uribe, F.; Wilson, W.; Pivovar, B. *ECS Transactions* **2007,** *11*, 383.